ADAR1 prevents autoinflammation by suppressing spontaneous ZBP1 activation

Richard de Reuver[1,2,9], Simon Verdonck[1,2,9], Evelien Dierick[1,2], Josephine Nemegeer[1,2], Eline Hessmann[1,2], Sadeem Ahmad[3,4], Maude Jans[1,2], Gillian Blancke[1,8], Filip Van Nieuwerburgh[5,6], Alexander Botzki[7], Lars Vereecke[1,8], Geert van Loo[1,2], Wim Declercq[1,2], Sun Hur[3,4], Peter Vandenabeele[1,2] and Jonathan Maelfait[1,2,*]

[1]VIB-UGent Center for Inflammation Research, 9052 Ghent, Belgium.

[2]Department of Biomedical Molecular Biology, Ghent University, 9052 Ghent, Belgium.

[3]Department of Biological Chemistry and Molecular Pharmacology, Harvard Medical School, Howard Hughes Medical Institute, Boston, MA 02115, USA.

[4]Program in Cellular and Molecular Medicine, Boston Children's Hospital, Howard Hughes Medical Institute, Boston, MA 02115, USA.

[5]NXTGNT, Faculty of Pharmaceutical Sciences, Ghent University, 9000 Ghent, Belgium.

[6]Laboratory of Pharmaceutical Biotechnology, Faculty of Pharmaceutical Sciences, Ghent University, 9000 Ghent, Belgium.

[7]VIB Bioinformatics Core, VIB, 9052 Ghent, Belgium.

[8]Department of Internal Medicine and Pediatrics, Ghent University, Ghent, Belgium.

[9]These authors contributed equally.

*Corresponding author: jonathan.maelfait@irc.vib-ugent.be

The RNA editing enzyme Adenosine Deaminase Acting on RNA 1 (ADAR1) limits accumulation of endogenous immunostimulatory double-stranded (ds)RNA[1]. In humans, reduced ADAR1 activity causes the severe inflammatory disease Aicardi-Goutières Syndrome (AGS)[2]. In mice, complete loss of ADAR1 activity is embryonically lethal[3-6] while mutations similar to those found in patients with AGS cause autoinflammation[7-12]. Mechanistically, adenosine-to-inosine (A-to-I) base modification of endogenous dsRNA by ADAR1 prevents chronic overactivation of the dsRNA sensors MDA5 and PKR[3,7-10,13,14]. Here we show that ADAR1 additionally inhibits spontaneous activation of the left-handed Z-nucleic acid sensor ZBP1. Activation of ZBP1 elicits caspase-8-dependent apoptosis and MLKL-mediated necroptosis of ADAR1 deficient cells. ZBP1 contributes to the embryonic lethality of *Adar* knockout mice and drives early mortality and intestinal cell death in *Adar*/*Mavs* doubly deficient animals. The Z-nucleic acid binding Zα domain of ADAR1 is critically required to prevent ZBP1-mediated intestinal cell death and skin inflammation. The Zα domain of ADAR1 promotes A-to-I editing of endogenous Alu elements to prevent dsRNA formation through pairing of inverted Alu repeats, which can otherwise induce ZBP1 activation. This shows that recognition of Alu duplex RNA by ZBP1 may contribute to the pathological features of AGS resulting from loss of ADAR1 function.

ADAR1 is a negative regulator of ZBP1

ADAR1 deficient (*Adar*$^{-/-}$) mice develop an MDA5-mediated type I interferon (IFN-I) response, which causes death between embryonic days (E)11.5 and E12.5[3,5,6,13-15]. Genetic removal of MDA5 or the downstream signalling protein MAVS rescues the embryonic lethality of *Adar*$^{-/-}$ mice. However, ADAR1/MDA5 or ADAR1/MAVS doubly deficient animals still die during the first weeks after birth[13,14,16] (Fig. 1a). This suggests that ADAR1

limits spontaneous activation of other immune sensors. In addition to binding to dsRNA through three consecutive dsRNA-binding motifs, ADAR1 can also interact with left-handed dsRNA or dsDNA in the Z-conformation via its N-terminal Zα domain[17,18]. We therefore hypothesised that ADAR1 may additionally suppress activation of the Z-nucleic acid sensor ZBP1. To test this hypothesis, we generated *Adar*$^{-/-}$ *Mavs*$^{-/-}$ animals expressing ZBP1 containing two amino acid substitutions in the two amino-terminal Zα domains (N46A/Y50A in the first Zα1 domain and N122A/Y126A in the second Zα2 domain)[19], which impair ZBP1 binding to Z-nucleic acids (Extended Data Fig. 1a)[20,21]. Sanger sequencing on *Htr2c*, *Mad2l1* and *Rpa1* mRNA, known substrates of ADAR1[3,6], confirmed complete lack of ADAR1 activity in these mice (Extended Data Fig. 1b). Despite having a lower birth weight in comparison with ADAR1 proficient littermates, *Adar*$^{-/-}$ *Mavs*$^{-/-}$ *Zbp1*$^{Zα1α2/Zα1α2}$ pups gained weight more rapidly than *Adar*$^{-/-}$ *Mavs*$^{-/-}$ *Zbp1*$^{+/+ \text{ or } +/Zα1α2}$ animals (Extended Data Fig. 1c). Around half of the *Adar*$^{-/-}$ *Mavs*$^{-/-}$ *Zbp1*$^{Zα1α2/Zα1α2}$ mice survived until ~20 weeks of life, however, they remained smaller than their control littermates (Fig. 1a and Extended Data Fig. 1d). Spontaneous ZBP1 activation causes necroptotic cell death of keratinocytes or intestinal epithelium, resulting in sterile autoinflammation[22-26]. Moreover, intestinal homeostasis is disrupted in *Adar*$^{-/-}$ *Mavs*$^{-/-}$ mice[13,16]. Since *Adar*$^{-/-}$ *Mavs*$^{-/-}$ mice did not develop skin lesions, we asked whether ZBP1-mediated cell death causes intestinal dysfunction in *Adar*/*Mavs* double knockouts. TdT-mediated dUTP nick end-labelling (TUNEL) revealed mild cell death in the ileum of 1 week old *Adar*/*Mavs* double knockouts mice that express wild type ZBP1, which was completely absent in ilea from *Adar*$^{-/-}$ *Mavs*$^{-/-}$ *Zbp1*$^{Zα1α2/Zα1α2}$ animals (Extended Data Fig. 1e,f). At 5 weeks of age, however, the ileum of *Adar*$^{-/-}$ *Mavs*$^{-/-}$ *Zbp1*$^{Zα1α2/Zα1α2}$ mice accumulated a substantial amount of dead cells. In contrast, colon tissues from 5 week old *Adar*$^{-/-}$ *Mavs*$^{-/-}$ *Zbp1*$^{Zα1α2/Zα1α2}$ were completely devoid of TUNEL-positive cells, while colons of 1 week *Adar*$^{-/-}$ *Mavs*$^{-/-}$ *Zbp1*$^{+/Zα1α2}$ animals displayed extensive cell death (Fig. 1b,c). The

differential phenotypic rescue across the intestine is consistent with the redundant role of ZBP1 in the ileum and its non-redundant role in the colon[27]. ADAR1 deficiency results in impaired neutrophil, T cell and B cell development, which occurs independently of MDA5/MAVS[13,16,28]. We confirmed that spleens of newborn *Adar*$^{-/-}$ *Mavs*$^{-/-}$ pups had reduced overall cellularity and contained less T and B cells albeit independently of the *Zbp1* genotype (Extended Data Fig. 2a,d). However, *Adar*$^{-/-}$ *Mavs*$^{-/-}$ *Zbp1*$^{+/+ \text{ or } +/Z\alpha1\alpha2}$ mice had almost no neutrophils and this phenotype was restored in mice expressing Zα domain mutant ZBP1, even in animals that reached 20 weeks of age (Extended Data Fig. 2a-c and Extended Data Fig 3b,c). In agreement with previous results showing that disrupted erythroid development due to loss of ADAR1 function was driven by MDA5/MAVS signalling[3,15,29], we observed normal red blood cell development in *Adar*$^{-/-}$ *Mavs*$^{-/-}$ *Zbp1*$^{Z\alpha1\alpha2/Z\alpha1\alpha2}$ mice although white blood cell counts were severely lowered (Extended Data Fig. 3a-c). This decrease was caused by a specific loss of lymphoid cells including B cells, T cells and NK(T) cells, while absolute numbers of myeloid cells remained unaffected (Extended Data Fig. 3b,c). This shows that spontaneous ZBP1 activation in *Adar*/*Mavs* double knockout mice results in intestinal cell death and impaired neutrophil development, while progressive loss of lymphoid cells occurs independently of MDA5/MAVS and ZBP1 and is possibly driven by other dsRNA sensors such as PKR and/or OAS proteins[30].

To test whether ZBP1 contributed to the embryonic death of ADAR1 deficient embryos, we monitored the viability of *Adar*$^{-/-}$ *Zbp1*$^{Z\alpha1\alpha2/Z\alpha1\alpha2}$ embryos at different stages during development (Extended Data Fig. 3e). In contrast to *Adar*$^{-/-}$ *Zbp1*$^{+/+}$ embryos, which had all died at E12.5, most *Adar*$^{-/-}$ *Zbp1*$^{Z\alpha1\alpha2/Z\alpha1\alpha2}$ appeared normal and ~80% of the embryos were still alive (Fig. 1d,e). *Adar*$^{-/-}$ embryos displayed a ZBP1-independent IFN-I response and increased expression of inflammatory genes (Extended Data Fig. 3d,f,g). We recovered only one *Adar*$^{-/-}$ *Zbp1*$^{Z\alpha1\alpha2/Z\alpha1\alpha2}$ embryo at E13.5, which was not viable (Extended Data Fig. 3e),

showing that loss of ZBP1 function extended the lifespan of these embryos by a maximum of one gestational day.

The Zα domain of ADAR1 limits ZBP1 activation

The Zα domain-containing p150 isoform of ADAR1, but not the p110 isoform, inhibits MDA5/MAVS-mediated immune activation and lethality in mice[13,31]. To determine whether the Zα-domain of ADAR1-p150 is physiologically important to limit spontaneous ZBP1 activation, we tested whether ZBP1 contributed to the pathogenesis of *Adar* knock-in mice that carry an *Adar* allele coding for an ADAR1 protein in which the Zα domain was mutated (N175A/Y179A, $Adar^{Z\alpha}$) paired with a second *Adar* null allele. As shown previously[10], all $Adar^{Z\alpha/-}$ $Zbp1^{+/+}$ animals died within 2 days, while over half of the $Adar^{Z\alpha/-}$ $Zbp1^{Z\alpha1\alpha2/Z\alpha1\alpha2}$ mice reached at least 18 weeks of age (Fig. 2a and Extended Data Fig. 4a). The surviving mice remained smaller compared to their *Adar* wild type littermates (Extended Data Fig. 4b,c). Caeca and colons of newborn $Adar^{Z\alpha/-}$ mice contained aggregates of necrotic tissue, which was absent in $Adar^{Z\alpha/-}$ $Zbp1^{Z\alpha1\alpha2/Z\alpha1\alpha2}$ pups (Extended Data Fig. 4d). In accordance, we detected TUNEL positive cells in the intestines of $Adar^{Z\alpha/-}$ mice, which was reduced in a ZBP1 Zα domain mutant background (Fig. 2b,c). RT-qPCR analysis of ISGs and inflammatory genes in intestinal, brain and lung tissues showed that ZBP1 partially contributed to the elevated expression of a subset of ISGs and inflammatory genes (Fig. 2d and Extended Data Fig. 4e,f). As such, ZBP1 may directly regulate the expression of specific ISGs and inflammatory genes. Alternatively, ZBP1-mediated cell death may indirectly contribute to the elevated expression of these genes through the release of DAMPs from dying cells and subsequent activation of other immune sensors. In contrast to the partial rescue of $Adar^{Z\alpha/-}$ $Zbp1^{Z\alpha1\alpha2/Z\alpha1\alpha2}$ mice, crossing $Adar^{Z\alpha/-}$ mice into a MAVS deficient background completely prevented intestinal cell death and the induction of ISG expression including

ZBP1 (Fig. 2b-d and Extended Data 4e), which is in line with the complete rescue of *Adar*$^{Zα/-}$ *Mavs*$^{-/-}$ mice from lethality[10]. Moreover, the survival of *Adar*$^{Zα/-}$ *Zbp1*$^{Zα1α2/Zα1α2}$ mice was much more pronounced in a *Mavs* heterozygous state (Extended Data Fig. 4g). This indicates that MAVS signalling potentiates ZBP1-induced pathology in *Adar*$^{Zα/-}$ mice, most likely by inducing expression of *Zbp1* itself.

To further validate whether Z-nucleic acid binding to ADAR1 is critical in restricting ZBP1 activation we crossed ADAR1 Zα domain mutant mice to keratinocyte-specific RIPK1 knockout animals (*Ripk1*^{EKO}). Others and we showed that recognition of endogenous Z-nucleic acids by ZBP1 causes RIPK3/MLKL-mediated necroptosis of RIPK1 deficient keratinocytes resulting in skin inflammation[22,23]. We did not retrieve any homozygous *Adar*$^{Zα/Zα}$ *Ripk1*^{EKO} animals suggesting that this gene combination was lethal *in utero*. The introduction of only one Zα domain mutant *Adar* allele in the *Ripk1*^{EKO} background, however, accelerated development of macroscopically visible skin lesions, enhanced thickening of the epidermis and increased influx of in the inflammatory cells (Fig. 2e-g and Extended Data Figs. 5a,b and 6). Together, these data demonstrate that an intact Zα domain of ADAR1 is crucial for inhibiting spontaneous ZBP1 activation.

ADAR1 inhibits ZBP1-induced cell death

Virus-induced ZBP1 activation leads to the recruitment of RIPK3, which induces parallel pathways of RIPK1/FADD/Caspase-8-mediated apoptosis and MLKL-mediated necroptosis[32,33]. To determine which signalling pathways cause death of ADAR1 deficient cells we treated primary murine lung fibroblasts with IFN-α to induce ZBP1 expression. To exclude confounding effects of spontaneous MDA5/MAVS and/or TNF signalling on cell survival we cultured *Adar*/*Mavs* double knockout cells with TNF neutralising antibodies. Stimulation of ADAR1-deficient fibroblasts with IFN-α and the protein synthesis inhibitor

cycloheximide (CHX), which sensitises to TNF-induced cell death by preventing translation of $cFLIP_L$[34,35], induced ZBP1-mediated cell death (Fig. 3a, Extended Data Fig. 7a). Western blotting revealed that ZBP1 induced both proteolytic activation of caspase-8 and phosphorylation of MLKL (Fig. 3b). This shows that CHX treatment sensitises ADAR1-deficient fibroblasts to ZBP1-mediated apoptosis and necroptosis, which may be held in check by the anti-apoptotic and anti-necroptotic functions of $cFLIP_L$[36,37]. Caspase-8 inhibition sensitises cells to ZBP1-mediated necroptosis[19,23]. Accordingly, treatment of IFN-α pre-stimulated fibroblasts with the pan-caspase inhibitor zVAD-fmk greatly accelerated ZBP1-dependent necroptosis of *Adar* knockout cells (Extended Data Fig. 7b,c) and in lung fibroblasts isolated from $Adar^{Z\alpha/-}$ $Mavs^{-/-}$ mice, which hemizygously express Zα domain mutant ADAR1 (Extended Data Fig. 7g,h). In contrast, ZBP1 activation after infection with herpes simplex virus 1 (HSV1) expressing a RIP homotypic interaction motif (RHIM)-mutant ICP6 protein, which is unable to block ZBP1-driven necroptosis[38], induced ZBP1-mediated necroptosis independently of ADAR1 (Extended Data Fig. 7d). As controls, apoptosis and necroptosis induced by TNF/CHX or TNF/zVAD-fmk proceeded independently from the *Adar* and/or *Zbp1* genotypes (Extended Data Fig. 7e,f,i,j). Intestinal crypts of $Adar^{Z\alpha/-}$ mice, both not of those expressing Zα domain mutant ZBP1 stained positive for cleaved caspase-8, confirming that reduced ADAR1 activity causes ZBP1-induced caspase-8 activation *in vivo* (Fig. 3c and Extended Data Fig 9a).

To explore these findings in human cells, we used siRNAs to deplete ADAR1 or only the Zα domain-containing ADAR1-p150 isoform (Extended Data Fig. 8a) in HT-29 colorectal adenocarcinoma lines transduced with either wild type human ZBP1 or Zα domain mutant ZBP1 (N46A/Y50A in the first Zα1 domain and N141A/Y145A in the second Zα2 domain). Consistent with the mouse data, ADAR1 depletion triggered death of cells expressing wild type ZBP1, but not of those expressing Zα-domain mutant ZBP1 (Extended Data Fig. 8b). As

controls, caspase-8-mediated apoptosis induced by TNF/CHX and necroptosis induced by combined treatment with TNF, the SMAC mimetic BV6 and zVAD-fmk proceeded with similar kinetics in both cell lines (Extended Data Fig. 8c,d). Specific depletion of ADAR1-p150 caused ZBP1-mediated cell death with similar kinetics as combined ADAR1-p110/p150 depletion, indicating that the p150 isoform is the main inhibitor of ZBP1 activation (Fig. 3d and Extended Data Fig. 8b,e). Treatment with zVAD-fmk inhibited cell death demonstrating that ADAR1(-p150) depletion in human cells elicited ZBP1-dependent apoptosis. This is further supported by the presence of cleaved caspase-8 (Fig. 3d,e and Extended Data Fig. 8e,f). Prolonged zVAD-fmk treatment caused a switch from apoptosis to necroptosis after *ADAR(-p150)*-specific siRNA transfection as shown by MLKL phosphorylation and by inhibition by the RIPK3 kinase inhibitor GSK'840 (Fig 3d,e and Extended Data Fig. 8e,f). Sole inhibition of RIPK3 by GSK'840 treatment without zVAD-fmk had no effect on cell death following ADAR1(-p150) depletion, revealing that the primary mode of cell death downstream of human ZBP1 is apoptosis. The RHIM-containing proteins RIPK1, RIPK3 but not TRIF (*TICAM1*), contributed to caspase-8-mediated apoptosis caused by ADAR1-p150 depletion in human ZBP1-expressing cells (Extended Data Fig. 8g,h). In sum, these data demonstrate that the Z-nucleic acid binding p150 isoform of ADAR1 limits ZBP1-mediated cell death in mouse and human cells.

Given the central role of RIPK3 in the induction of ZBP1-mediated caspase-8-dependent apoptosis and MLKL-dependent necroptosis during virus infection[32,33], we generated $Adar^{Z\alpha/-}$ mice in a RIPK3 deficient background. As opposed to the prolonged survival of $Adar^{Z\alpha/-}$ $Zbp1^{Z\alpha1\alpha2/Z\alpha1\alpha2}$ animals (see Fig. 2a), we observed only a minor survival advantage by genetic removal of one or two *Ripk3* alleles (Extended Data Fig 9b,c). In the absence of RIPK3, ZBP1 may directly recruit RIPK1 to induce caspase-8-mediated apoptosis[32,33]. We therefore crossed $Adar^{Z\alpha/-}$ animals into a MLKL/caspase-8 doubly deficient background to abrogate both the

necroptotic and the extrinsic apoptotic pathways. Surprisingly, none of the resulting *Adar*$^{Zα/-}$ *Mlkl*$^{-/-}$ *Casp8*$^{-/-}$ mice survived beyond 2 days of birth (Extended Data Fig 8d-h). While intestinal cell death was reduced in *Adar*$^{Zα/-}$ *Zbp1*$^{Zα1α2/Zα1α2}$ mice (see Fig. 2b), we still detected substantial TUNEL positive cells in the colons of *Adar*$^{Zα/-}$ *Mlkl*$^{-/-}$ *Casp8*$^{-/-}$ pups (Fig. 3f,g). Future studies will address how these mice are not rescued from lethality. It is possible that ZBP1 directly activates other cell death pathways or that caspase-8 and/or MLKL dampen(s) death signals that originate from or other immune sensors in *Adar*$^{Zα/-}$ mice.

Alu duplex RNA activates ZBP1

To understand how loss of Zα domain-dependent ADAR1 functions cause spontaneous activation of ZBP1, we performed high-coverage mRNA sequencing to analyse the A-to-I editing profile of repeat elements within mRNA transcripts in ADAR1 Zα domain mutant mouse fibroblasts and human HEK293 cells[10]. We used primary lung fibroblasts from *Adar*$^{Zα/-}$ *Mavs*$^{-/-}$ mice to minimise the effects of differential expression due to spontaneous MDA5/MAVS activation. Cells were stimulated with IFN-α to induce ADAR1-p150 expression and editing by this isoform. As expected, IFN-α stimulation increased overall editing of repeats in mouse fibroblasts (Extended Data Fig. 10a). Mouse SINE/Alu, B2 and B4 elements and human Alu repeats made up the majority of edited repeat elements (Fig. 4b Extended and Data 10b). In contrast to previous studies reporting that a subset of editing sites may be specifically regulated by Zα domain of ADAR1[8-10] our high coverage approach, which allowed us to detect also sparsely edited adenosines across whole repeat sequences, did not reveal a substantial ADAR1 genotype-dependent bias in A-to-I editing (Fig. 4b and Extended Data Fig. 10c). Instead, loss of Zα domain-mediated interactions of ADAR1 with Z-nucleic acids led to an overall reduction in the quality of repeat editing (Fig. 4a,c). Complete editing of an AluSp element that was most significantly affected by ADAR1 Zα domain

mutation and its nearest inverted AluSx1 repeat created 11 more bulges within the predicted AluSp:AluSx1 RNA duplex and substantially lowered its stability (Fig. 4c and Extended Data Fig. 10d-f). Alu:Alu hybrids are potent agonists of MDA5 when ADAR1 activity is lost[39,40]. To test whether these dsRNA structures could also stimulate ZBP1, we transfected *in vitro* transcribed Alu:Alu hybrids from the 3'UTRs of the *NICN1* and *BPNT1* mRNAs into HT-29 cells expressing human ZBP1. Both Alu:Alu hybrids potently induced ZBP1-dependent cell death, which depended on intact ZBP1 Zα domains and which could be inhibited by zVAD-fmk (Fig. 4d,e and Extended Data Fig. 10g). Similar to the siRNA-mediated ADAR1 depletion experiments (see Fig. 3d and Extended Data Fig. 8e), prolonged ZBP1 stimulation and caspase blockade triggered a cell death that could be blocked by the RIPK3 kinase inhibitor GSK'840 (Fig. 4e and Extended Data Fig. 10g).

Discussion

Collectively, we demonstrate that ADAR1 is a negative regulator of ZBP1-mediated apoptosis and necroptosis, which is in line with a recent study showing that loss of ADAR1 sensitises to ZBP1-induced cell death caused by nuclear export inhibition[41]. The P193A mutation within the Zα domain of ADAR1 causes AGS when paired with an ADAR null allele[2]. Our study in *Adar*$^{Zα/-}$ mice, which mimic these compound heterozygous mutations, shows that ZBP1 may contribute to AGS pathology[7]. It is conceivable that bilateral striatal necrosis, a phenotype that uniquely manifests in patients with AGS caused by *ADAR* mutations and involves an acute loss of neurons[42], is triggered by ZBP1-mediated cell death of neuronal cells. Finally, this study implicating ZBP1 as a sensor for endogenous Alu duplex RNA, along with recent studies showing that ZBP1 acts as a dsRNA sensor during virus infection[43,44], further substantiates the concept that ZBP1 constitutes an integral part of the mammalian dsRNA response.

References

1 Samuel, C. E. Adenosine deaminase acting on RNA (ADAR1), a suppressor of double-stranded RNA-triggered innate immune responses. *J Biol Chem* **294**, 1710-1720, doi:10.1074/jbc.TM118.004166 (2019).

2 Rice, G. I. *et al.* Mutations in ADAR1 cause Aicardi-Goutieres syndrome associated with a type I interferon signature. *Nat Genet* **44**, 1243-1248, doi:10.1038/ng.2414 (2012).

3 Liddicoat, B. J. *et al.* RNA editing by ADAR1 prevents MDA5 sensing of endogenous dsRNA as nonself. *Science* **349**, 1115-1120, doi:10.1126/science.aac7049 (2015).

4 Ward, S. V. *et al.* RNA editing enzyme adenosine deaminase is a restriction factor for controlling measles virus replication that also is required for embryogenesis. *Proc Natl Acad Sci U S A* **108**, 331-336, doi:10.1073/pnas.1017241108 (2011).

5 Wang, Q. *et al.* Stress-induced apoptosis associated with null mutation of ADAR1 RNA editing deaminase gene. *J Biol Chem* **279**, 4952-4961, doi:10.1074/jbc.M310162200 (2004).

6 Hartner, J. C. *et al.* Liver disintegration in the mouse embryo caused by deficiency in the RNA-editing enzyme ADAR1. *J Biol Chem* **279**, 4894-4902, doi:10.1074/jbc.M311347200 (2004).

7 Maurano, M. *et al.* Protein kinase R and the integrated stress response drive immunopathology caused by mutations in the RNA deaminase ADAR1. *Immunity* **54**, 1948-1960 e1945, doi:10.1016/j.immuni.2021.07.001 (2021).

8 Nakahama, T. *et al.* Mutations in the adenosine deaminase ADAR1 that prevent endogenous Z-RNA binding induce Aicardi-Goutieres-syndrome-like encephalopathy. *Immunity* **54**, 1976-1988 e1977, doi:10.1016/j.immuni.2021.08.022 (2021).

9 Tang, Q. *et al.* Adenosine-to-inosine editing of endogenous Z-form RNA by the deaminase ADAR1 prevents spontaneous MAVS-dependent type I interferon responses. *Immunity* **54**, 1961-1975 e1965, doi:10.1016/j.immuni.2021.08.011 (2021).

10 de Reuver, R. *et al.* ADAR1 interaction with Z-RNA promotes editing of endogenous double-stranded RNA and prevents MDA5-dependent immune activation. *Cell Rep* **36**, 109500, doi:10.1016/j.celrep.2021.109500 (2021).

11 Guo, X. *et al.* Aicardi-Goutieres syndrome-associated mutation at ADAR1 gene locus activates innate immune response in mouse brain. *J Neuroinflammation* **18**, 169, doi:10.1186/s12974-021-02217-9 (2021).

12 Inoue, M. *et al.* An Aicardi-Goutieres Syndrome-Causative Point Mutation in Adar1 Gene Invokes Multiorgan Inflammation and Late-Onset Encephalopathy in Mice. *J Immunol*, doi:10.4049/jimmunol.2100526 (2021).

13 Pestal, K. *et al.* Isoforms of RNA-Editing Enzyme ADAR1 Independently Control Nucleic Acid Sensor MDA5-Driven Autoimmunity and Multi-organ Development. *Immunity* **43**, 933-944, doi:10.1016/j.immuni.2015.11.001 (2015).

14 Mannion, N. M. *et al.* The RNA-editing enzyme ADAR1 controls innate immune responses to RNA. *Cell Rep* **9**, 1482-1494, doi:10.1016/j.celrep.2014.10.041 (2014).

15 Hartner, J. C., Walkley, C. R., Lu, J. & Orkin, S. H. ADAR1 is essential for the maintenance of hematopoiesis and suppression of interferon signaling. *Nat Immunol* **10**, 109-115, doi:10.1038/ni.1680 (2009).

16 Bajad, P. *et al.* An internal deletion of ADAR rescued by MAVS deficiency leads to a minute phenotype. *Nucleic Acids Res* **48**, 3286-3303, doi:10.1093/nar/gkaa025 (2020).

17 Placido, D., Brown, B. A., 2nd, Lowenhaupt, K., Rich, A. & Athanasiadis, A. A left-handed RNA double helix bound by the Z alpha domain of the RNA-editing enzyme ADAR1. *Structure* **15**, 395-404, doi:10.1016/j.str.2007.03.001 (2007).
18 Schwartz, T., Rould, M. A., Lowenhaupt, K., Herbert, A. & Rich, A. Crystal structure of the Zalpha domain of the human editing enzyme ADAR1 bound to left-handed Z-DNA. *Science* **284**, 1841-1845, doi:10.1126/science.284.5421.1841 (1999).
19 Maelfait, J. *et al.* Sensing of viral and endogenous RNA by ZBP1/DAI induces necroptosis. *EMBO J* **36**, 2529-2543, doi:10.15252/embj.201796476 (2017).
20 Deigendesch, N., Koch-Nolte, F. & Rothenburg, S. ZBP1 subcellular localization and association with stress granules is controlled by its Z-DNA binding domains. *Nucleic Acids Res* **34**, 5007-5020, doi:10.1093/nar/gkl575 (2006).
21 Feng, S. *et al.* Alternate rRNA secondary structures as regulators of translation. *Nat Struct Mol Biol* **18**, 169-176, doi:10.1038/nsmb.1962 (2011).
22 Devos, M. *et al.* Sensing of endogenous nucleic acids by ZBP1 induces keratinocyte necroptosis and skin inflammation. *J Exp Med* **217**, doi:10.1084/jem.20191913 (2020).
23 Jiao, H. *et al.* Z-nucleic-acid sensing triggers ZBP1-dependent necroptosis and inflammation. *Nature* **580**, 391-395, doi:10.1038/s41586-020-2129-8 (2020).
24 Wang, R. *et al.* Gut stem cell necroptosis by genome instability triggers bowel inflammation. *Nature* **580**, 386-390, doi:10.1038/s41586-020-2127-x (2020).
25 Kesavardhana, S. *et al.* The Zalpha2 domain of ZBP1 is a molecular switch regulating influenza-induced PANoptosis and perinatal lethality during development. *J Biol Chem* **295**, 8325-8330, doi:10.1074/jbc.RA120.013752 (2020).
26 Ingram, J. P. *et al.* ZBP1/DAI Drives RIPK3-Mediated Cell Death Induced by IFNs in the Absence of RIPK1. *J Immunol* **203**, 1348-1355, doi:10.4049/jimmunol.1900216 (2019).
27 Schwarzer, R., Jiao, H., Wachsmuth, L., Tresch, A. & Pasparakis, M. FADD and Caspase-8 Regulate Gut Homeostasis and Inflammation by Controlling MLKL- and GSDMD-Mediated Death of Intestinal Epithelial Cells. *Immunity* **52**, 978-993 e976, doi:10.1016/j.immuni.2020.04.002 (2020).
28 Vongpipatana, T., Nakahama, T., Shibuya, T., Kato, Y. & Kawahara, Y. ADAR1 Regulates Early T Cell Development via MDA5-Dependent and -Independent Pathways. *J Immunol* **204**, 2156-2168, doi:10.4049/jimmunol.1900929 (2020).
29 Liddicoat, B. J. *et al.* Adenosine-to-inosine RNA editing by ADAR1 is essential for normal murine erythropoiesis. *Exp Hematol* **44**, 947-963, doi:10.1016/j.exphem.2016.06.250 (2016).
30 Hur, S. Double-Stranded RNA Sensors and Modulators in Innate Immunity. *Annu Rev Immunol* **37**, 349-375, doi:10.1146/annurev-immunol-042718-041356 (2019).
31 Kim, J. I. *et al.* RNA editing at a limited number of sites is sufficient to prevent MDA5 activation in the mouse brain. *PLoS Genet* **17**, e1009516, doi:10.1371/journal.pgen.1009516 (2021).
32 Kuriakose, T. *et al.* ZBP1/DAI is an innate sensor of influenza virus triggering the NLRP3 inflammasome and programmed cell death pathways. *Sci Immunol* **1**, doi:10.1126/sciimmunol.aag2045 (2016).
33 Thapa, R. J. *et al.* DAI Senses Influenza A Virus Genomic RNA and Activates RIPK3-Dependent Cell Death. *Cell Host Microbe* **20**, 674-681, doi:10.1016/j.chom.2016.09.014 (2016).

34 Kreuz, S., Siegmund, D., Scheurich, P. & Wajant, H. NF-kappaB inducers upregulate cFLIP, a cycloheximide-sensitive inhibitor of death receptor signaling. *Mol Cell Biol* **21**, 3964-3973, doi:10.1128/MCB.21.12.3964-3973.2001 (2001).
35 Micheau, O., Lens, S., Gaide, O., Alevizopoulos, K. & Tschopp, J. NF-kappaB signals induce the expression of c-FLIP. *Mol Cell Biol* **21**, 5299-5305, doi:10.1128/MCB.21.16.5299-5305.2001 (2001).
36 Dillon, C. P. *et al.* Survival function of the FADD-CASPASE-8-cFLIP(L) complex. *Cell Rep* **1**, 401-407, doi:10.1016/j.celrep.2012.03.010 (2012).
37 Oberst, A. *et al.* Catalytic activity of the caspase-8-FLIP(L) complex inhibits RIPK3-dependent necrosis. *Nature* **471**, 363-367, doi:10.1038/nature09852 (2011).
38 Guo, H. *et al.* Species-independent contribution of ZBP1/DAI/DLM-1-triggered necroptosis in host defense against HSV1. *Cell Death Dis* **9**, 816, doi:10.1038/s41419-018-0868-3 (2018).
39 Ahmad, S. *et al.* Breaching Self-Tolerance to Alu Duplex RNA Underlies MDA5-Mediated Inflammation. *Cell* **172**, 797-810 e713, doi:10.1016/j.cell.2017.12.016 (2018).
40 Chung, H. *et al.* Human ADAR1 Prevents Endogenous RNA from Triggering Translational Shutdown. *Cell* **172**, 811-824 e814, doi:10.1016/j.cell.2017.12.038 (2018).
41 Karki, R. *et al.* ADAR1 restricts ZBP1-mediated immune response and PANoptosis to promote tumorigenesis. *Cell Rep* **37**, 109858, doi:10.1016/j.celrep.2021.109858 (2021).
42 Livingston, J. H. *et al.* A type I interferon signature identifies bilateral striatal necrosis due to mutations in ADAR1. *J Med Genet* **51**, 76-82, doi:10.1136/jmedgenet-2013-102038 (2014).
43 Koehler, H. *et al.* Vaccinia virus E3 prevents sensing of Z-RNA to block ZBP1-dependent necroptosis. *Cell Host Microbe* **29**, 1266-1276 e1265, doi:10.1016/j.chom.2021.05.009 (2021).
44 Zhang, T. *et al.* Influenza Virus Z-RNAs Induce ZBP1-Mediated Necroptosis. *Cell* **180**, 1115-1129 e1113, doi:10.1016/j.cell.2020.02.050 (2020).

Figures

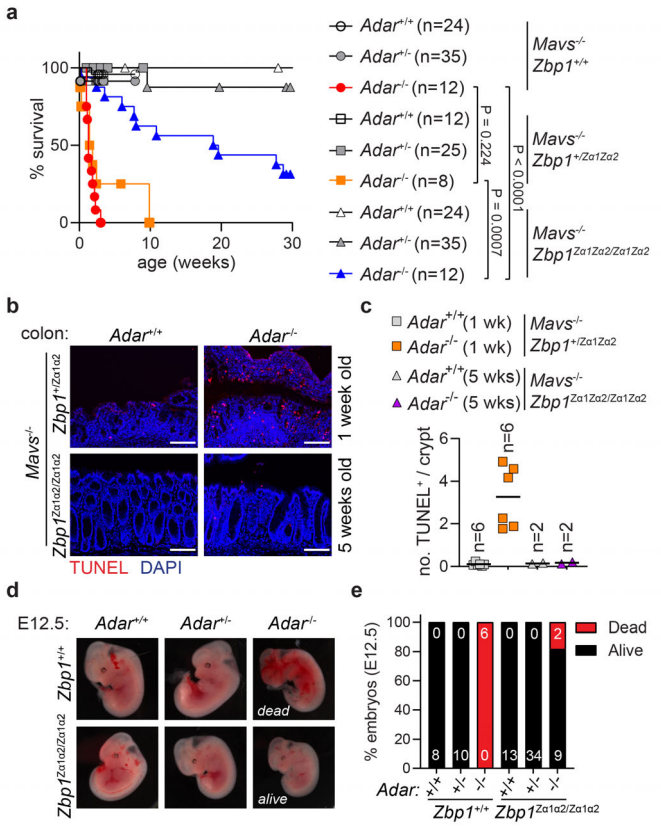

Fig. 1. ZBP1 causes early postnatal lethality of *Adar/Mavs* double knockout mice and accelerates death of *Adar*$^{-/-}$ embryos. a, Kaplan-Meier survival curve of mice from the indicated genotypes. P values by log-rank test. The numbers of mice (n) that were analysed per genotype are indicated in the graph. **b,c,** TUNEL assay on colon sections from 1 or 5 week old *Adar*$^{-/-}$ *Mavs*$^{-/-}$ mice expressing Zα domain mutant ZBP1 from one (*Zbp1*$^{+/Zα1α2}$) or two (*Zbp1*$^{Zα1α2/Zα1α2}$) alleles. Representative images of colon sections are shown in **(b)**. Scale bar = 100 µm. Quantification **(c)** of TUNEL^{+} cells per crypt. Lines represent the mean; each data point represents an individual mouse; numbers of mice (n) that were analysed per genotype are indicated in the graph. **d,** Macroscopic pictures of E12.5 embryos of the indicated genotypes. **e,** Viability of E12.5 embryos based on the presence/absence of a heartbeat. Numbers in the bar chart represent the number of embryos that were analysed per genotype.

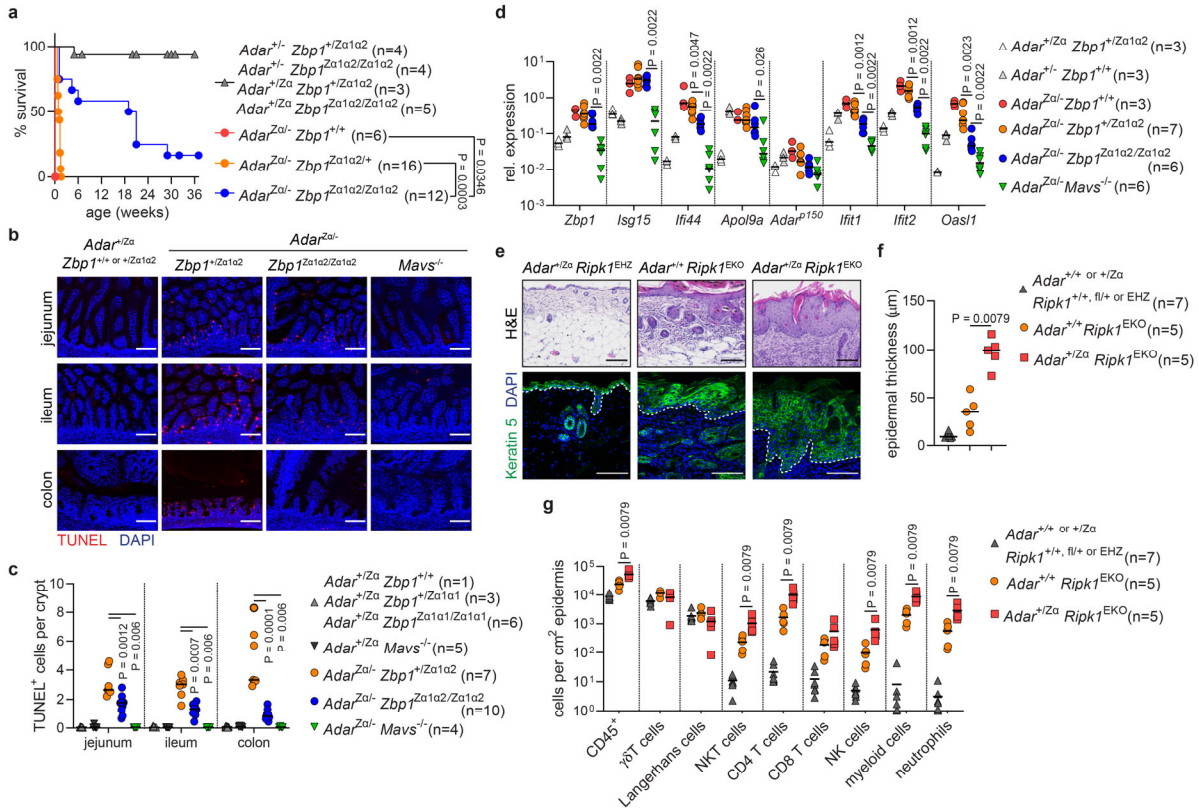

Figure 2. The Zα domain of ADAR1-p150 is critical in preventing spontaneous ZBP1 activation. a, Kaplan-Meier survival curve of mice from the indicated genotypes. P values by log-rank test. The numbers of mice (n) that were analysed per genotype are indicated in the graph. **b,c,** TUNEL assay on intestinal tissue sections from the jejunum, ileum and colon of 1 day old pups from the indicated genotypes. Representative images of jejunum, ileum and colon sections are shown in **(b)**. Scale bar = 100 µm. Quantification **(c)** of TUNEL^{+} cells per crypt. **d,** RT-qPCR analysis of the indicated ISGs, analysed in whole intestine samples of 1 day old pups of the indicated genotypes. **e-g,** Skin analysis of epidermis-specific RIPK1 knockout mice (*Ripk1*^{EKO}) carrying heterozygous ADAR1 Zα domain mutant alleles (*Adar*$^{+/Zα}$) or expressing wild type ADAR1. Littermate offspring containing one or two functional *Ripk1* alleles (*Ripk1*$^{+/+,\ fl/+}$) or heterozygously expressing a functional *Ripk1* allele in the epidermis (*Ripk1*^{EHZ}) did not develop lesions and are shown as controls. Skin sections of 21 day old mice were stained with H&E or Keratin 5 and DAPI **(e)**. Scale bar = 100 µm.

Quantification of epidermal thickness **(f)** on H&E-stained sections shown in **(e)**. Flow cytometry analysis **(g)** of leukocyte ($CD45^+$) composition of the epidermis of 21 day old mice of the indicated genotypes. Gating strategy is outlined in Extended Data Fig. 6. Lines in **(c,d,f,g)** represent the mean; each data point in **(c,d,f,g)** represents an individual mouse; numbers of mice (n) that were analysed per genotype are indicated in the graph; P values by Mann-Whitney test.

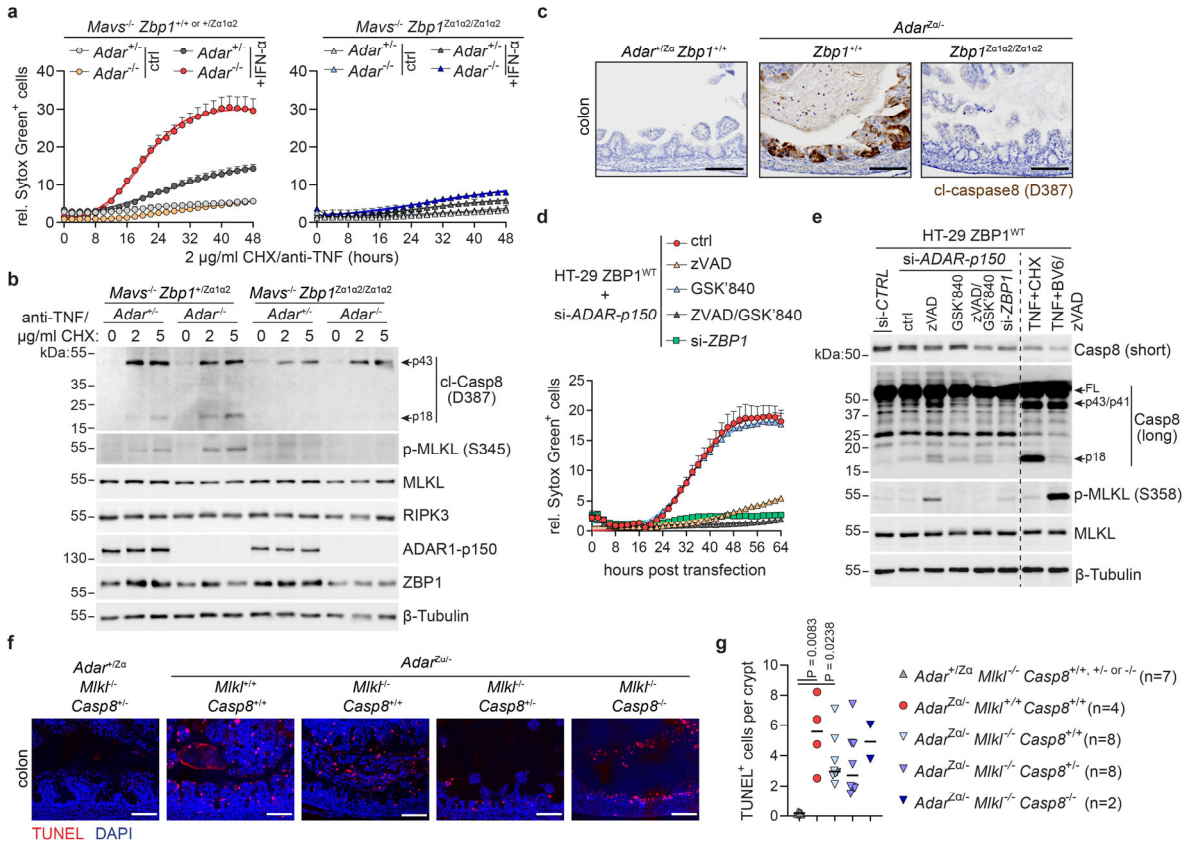

Fig. 3. Loss of ADAR1 function induces ZBP1-mediated caspase-8-dependent apoptosis and MLKL-dependent necroptosis. a,b Primary mouse lung fibroblasts of the indicated genotypes were stimulated with 200 U/mL IFN-α for 16 hours or left untreated (ctrl). Next, cells were treated with 2 µg/mL or 5 µg/mL CHX and 1 µg/mL anti-mouse TNF. Cell death was quantified by measuring relative (rel.) SYTOX Green uptake every 2 hours. **b,** Immunoblot related to **(a)** and Extended Data Fig. 7a. Samples were harvested 16 hours post treatment. **c,** Representative images of cleaved caspase-8 (D387) staining of colon sections of mice of the indicated genotypes. Scale bars = 100 µm. 3 mice per genotype were analysed. **d,e,** Human HT-29 cells stably expressing wild type human ZBP1 (ZBP1^{WT}) were transfected with control siRNAs (si-*CTRL*) or siRNAs targeting the p150 isoform of *ADAR* (si-*ADAR-p150*) and *ZBP1* (si-*ZBP1*). 5 hours later, cells were treated with 20 µM zVAD-fmk and/or 3 µM GSK'840. Cell death was analysed as in **(a)** and protein expression **(e)** was analysed at 30

hours post transfection. Controls samples were treated with 30 ng/mL human TNF, 5 μM BV6 and 20 μM zVAD-fmk for 3 hours or 30 ng/mL TNF and 20 μg/mL CHX for 6 hours. **f,g,** TUNEL assay on colon sections from 1 day old mice of the indicated genotypes. Representative images of colon sections are shown in **(f)** Scale bar = 100 μm. Quantification **(g)** of $TUNEL^+$ cells per crypt. Lines represent the mean; each data point represents an individual mouse; P values by Mann-Whitney test. Data in **(a,d)** are representative of 3 independent experiments; Fitted lines represent a logistic growth fit and data points show the mean + SEM. For gel source data, see Supplementary Figure 1.

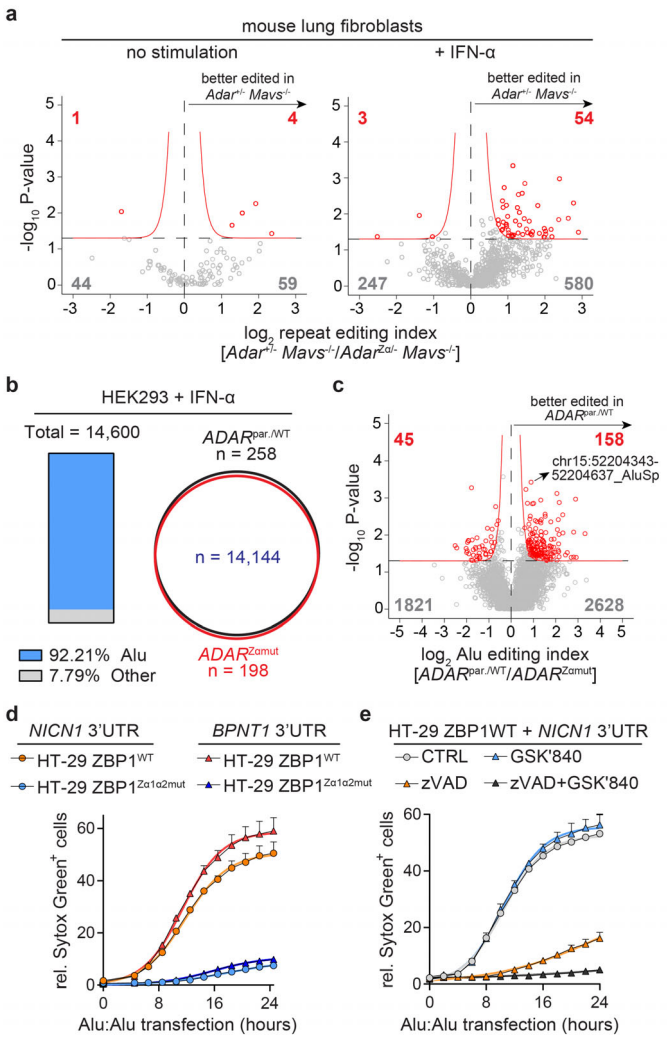

Fig. 4. Alu duplex RNA stimulates ZBP1-dependent cell death. a, Primary lung fibroblasts from *Adar*$^{+/-}$ *Mavs*$^{-/-}$ and *Adar*$^{Zα/-}$ *Mavs*$^{-/-}$ mice were stimulated for 16 hours with 200 U/mL IFN-α or left untreated. The repeat editing index was calculated using all identified A-to-I editing sites within a single repeat element. **b,** Wild type (HEK293 parental cells and 2 wild type clones; *ADAR*$^{par./WT}$) and *ADAR*^{Zαmut} HEK293 clones were stimulated for 16 hours with 1,000 U/mL IFN-α. Repeat families that underwent A-to-I editing in 3 independent HEK293 clones are visualised in the boxplot. The Venn diagram illustrates the number of repeat elements that displayed genotype specific A-to-I editing or those that were detected in both groups. **c,** Volcano plot demonstrating the differential A-to-I editing activity on Alu elements comparing wild type and *ADAR*^{Zαmut} HEK293 cells. The Alu editing index represents the

combined A-to-I editing efficiency calculated from detected editing sites belonging to the same Alu element. **d,** HT-29 cells stably expressing wild type ZBP1 ($ZBP1^{WT}$) or Zα domain mutant ZBP1 ($ZBP1^{Zα1Zα2mut}$) were transfected with 50 ng *NICN1* and *BPNT1* 3' UTR Alu duplex RNA. **e,** Transfection of HT-29 $ZBP1^{WT}$ with 50 ng of *NICN1* UTR duplex RNA in combination with 3 μM GSK'840 and/or 20 μM zVAD-fmk. Cell death in **(d,e)** was analysed as in Fig. 3d. Data in are representative of three independent experiments. Fitted lines represent a logistic growth fit and data points show the mean + SEM.

Methods

Mice

Adar$^{+/-}$ and *Adar*$^{Zα/Zα}$ mice[10] and *Zbp1*$^{Zα1α2/Zα1α2}$ mice[21] and were generated in C57Bl/6 ES cells and were previously described. *Mavs*$^{-/-}$ mice were obtained from J. Tschopp[45]. *Ripk3*$^{-/-}$ mice were obtained from V. Dixit[46]. *Mlkl*$^{-/-}$ *Casp8*$^{-/-}$ mice were generated by crossing an *Mlkl*$^{fl/fl}$ *Casp8*$^{fl/fl}$ male to a female Sox2-Cre deleter mouse[47] to generate *Mlkl*$^{+/-}$ *Casp8*$^{+/-}$ offspring. *Mlkl*$^{fl/fl}$ mice were obtained from J. Murphy[48] and *Casp8*$^{fl/fl}$ mice were obtained from S. Hedrick[49]. All alleles were maintained on a C57BL/6 genetic background. Mice were housed in individually ventilated cages at the VIB-UGent Center for Inflammation Research in a specific pathogen-free facility, according to national and institutional guidelines for animal care. Sequences of primers used for genotyping are listed in Supplementary Table 1. All experiments were conducted following approval by the local Ethics Committee of Ghent University.

Antibodies and reagents

Antibodies against the following proteins were used for Western blot analysis: ADAR1 (14175, Cell Signaling Technology), ADAR1-p150 (293003, Synaptic Systems GmbH; A303-883A, Bethyl), RIPK1 (3493, Cell Signaling Technology), RIPK3 (2283, ProSci Incorporated; 10188, Cell Signaling Technology), MLKL (MABC604, Millipore; GTX107538, GeneTex), p-MLKL (ab187091, Abcam; 37333, Cell Signaling Technology), ZBP1 (AG-20B-0010, Adipogen; 60968, Cell Signaling Technology), Caspase-8 (8592, Cell Signaling Technology), TRIF (4596; Cell Signaling Technology), MAVS (4983, Cell Signaling Technology) and β-Tubulin (ab21058, Abcam). Mouse anti-human Caspase-8 antibody was kindly provided by P.H. Krammer. The following secondary antibodies were

used for detection: donkey anti-rabbit IgG-HRP (NA934, GE Healthcare), sheep anti-mouse IgG-HRP (NA931, GE Healthcare) and goat anti-rat IgG (NA935, GE Healthcare).

The following fluorochrome-conjugated antibodies and dyes were used for flow cytometry analysis: PE-Cyanine5 CD19 (15-0193-82, Thermo Fisher Scientific), AlexaFluor700 CD19 (56-0193-80, Thermo Fisher Scientific), BUV395 CD3e (563565, BD Biosciences), PE-Cy7 CD11c (25-0114-82, Thermo Fisher Scientific), FITC MHC Class II (I-A/I-E) (11-5321-82, eBioscience), BV605 mouse anti-mouse CD161 (NK-1.1; 563220, BD Biosciences), PerCP-Cy5.5 rat anti-mouse CD11b (550993, BD Biosciences), APC-eFluor780 CD11b (47-0112-80, Thermo Fisher Scientific), BUV735 CD4 (564298, BD Biosciences), eFluor450 CD8a (48-0081-82, eBioscience), FITC CD8a (100705, BioLegend), PE XCR1 (148203, BioLegend), PerCP-eFluor710 CD172a (SIRP-α; 46-1721-82, eBioscience), BV785 Ly-6G (127645, BioLegend), APC-Cy7 Ly-6C (560596, BD Biosciences), BV711 CD64 (139311, BioLegend), AlexaFluor700 CD45 (56-0451-80, Thermo Fisher Scientific), BV421 Siglec-F (565934, BD Biosciences), PE CD200R3 (142205, BioLegend), APC-Cy7 TCR β chain (109220, BioLegend), APC F4/80 (17-4801, Thermo Fisher Scientific), PE-CF594 γδ TCR (563532, BD Biosciences), CD16/CD32 (Fc block; 553142, BD Biosciences), eFluor506 FVD (65-0866-14, Thermo Fisher Scientific).

Mouse and human TNF, mouse IFN-γ and mouse anti-TNF neutralising antibody (clone 1F3F3D4) were produced by the VIB protein Service Facility. Hybrid IFNα-B/D (CGP35269, Novartis), human IFN-α2 (592704, BioLegend), human IFN-γ (300-02, PeproTech), zVAD-fmk (BACEN-1510.0005, Bachem), CHX (C7698, Sigma-Aldrich), BV6 (S7597, Selleckchem). HSV1-ICP6^{mutRHIM} was a kind gift from J. Han[50].

Cell culture

HT-29 cells (ATCC HTB-38) were cultured at 37°C and 5% CO_2 in McCoy's 5a Medium (16600082, GIBCO) supplemented with 10% FCS (TICO Europe), 2 mM Glutamine (BE17-605F, Lonza) and 1mM sodium pyruvate (S8636, Sigma-Aldrich). HEK293T (ATCC CRL-3216) were cultured in high-glucose (4500 mg/liter) DMEM (41965–039, GIBCO) supplemented with 10% FCS (TICO Europe) and 2 mM glutamine (BE17-605F, Lonza).

For lentivirus production, HEK293T cells were transfected with C-terminally EGFP and V5-tagged wild-type human ZBP1 or Zα1α2-mutant human ZBP1 transducing vectors in the pDG2i backbone[51] together with the pCMV delta R8.91 gag-pol-expressing packaging plasmids and pMD2.G VSV-G-expressing envelope plasmid. 24 hours after transfection, medium was refreshed. 48 hours after transfection, the viral supernatant was harvested and used for transduction of 500,000 HT-29 cells seeded in 6-well plates in presence of 8 µg/mL polybrene (H9268, Sigma-Aldrich). The next day, medium was refreshed and two days later cells were seeded in a T75 flask in selection medium containing 2 µg/mL puromycin (P7255, Sigma-Aldrich). Transduced cells were sorted for EGFP expression on a FACSMelody Cell Sorter (BD Biosciences) and clones originating from single cells were established.

Primary lung fibroblasts were isolated from lungs of mice of the indicated genotypes. Lungs were sterilized with 70% ethanol before cutting the tissue in pieces of ~25mm. Digestion was performed with a 0.1% collagenase D (11088866001, Roche) and 0.2% trypsin solution (15090-046, GIBCO) for 30 min at 37°C. The collagenase D / trypsin solution was refreshed and digestion continued another 30 minutes at 37°C. After neutralization with αMEM-20 [αMEM (22571-020, GIBCO) supplemented with 20% FCS, 2mM glutamine (BE17-605F, Lonza), 1mM sodium pyruvate (S8636, Sigma-Aldrich), 100 U/ml penicillin and 100 µg/ml streptomycin (P4333, Sigma-Aldrich), cells were pelleted at 400 g for 5 min and resuspended in αMEM-20 culture medium. The purity of primary lung fibroblasts was assured by passaging each fibroblast line for at least 3 times in αMEM-20, which selectively supports

growth of fibroblasts, whereas other cell types die or stop proliferating. Primary murine lung fibroblasts were maintained under hypoxic conditions (3% O2 at 37°C and 5% CO2 in αMEM-20).

Western blotting

For Western blotting, cells were washed twice with ice-cold PBS and lysed in protein lysis buffer (50 mM Tris-HCl pH 7.5 (15567027, GIBCO), 1% Igepal CA-630 (I8896, Sigma-Aldrich), 150 mM NaCl and 10% glycerol (7122301, Biosolve) supplemented with complete protease inhibitor cocktail (11697498001, Roche) and PhosSTOP (4906845001, Roche). HT-29 cell lysates were cleared by centrifugation at 20,000 g for 10 minutes. Embryonic tissue and pPrimary mouse lung fibroblast lysates were cleared at 12,000 g for 20 minutes. 5x Laemmli loading buffer (250 mM Tris HCl, pH 6.8, 10% SDS, 0.5% Bromophenol blue, 50% glycerol, and 20% β-mercaptoethanol) was added to the supernatant. Finally, samples were incubated at 95°C for 5 min and analysed using Tris-Glycine SDS-PAGE and semi-dry immunoblotting.

RT-qPCR

For RT-qPCR, (embryonic) tissue was homogenised in Trizol reagent (15596-018, GIBCO) followed by phase separation with chloroform. Next, the aqueous layer was loaded onto Nucleospin RNA Plus columns (740984.250, Macherey-Nagel). cDNA synthesis was performed with the SensiFast cDNA synthesis kit (BIO-65054, Bioline). PrimeTime qPCR Master Mix (1055771, IDT) was used for cDNA amplification using a Lightcycler 480 system (Roche). Primers and probes (Taqman) used for quantitative reverse-transcription PCR in this study are listed in Supplementary Table 1.

Histology

Fixation of intestinal tissues occurred overnight at 4°C in 10% formalin. Next, samples were embedded in paraffin and sectioned at 5 µm thickness. H&E staining was performed using a Varistain Slide Stainer. H&E stained sections were imaged with a Zeiss Axio Scan slide scanner and further analysed with the Zeiss blue software. TdT-mediated dUTP nick end-labelling (TUNEL) staining was performed using the TMR red in situ cell death detection kit (12156792910, Sigma-Aldrich). All sections were counterstained with DAPI (D21490, Thermo Fisher Scientific). For immunohistochemistry, sections were deparaffinized and rehydrated using a Varistain Slide Stainer. Antigen retrieval was performed by boiling sections at 95°C for 10 min in antigen retrieval solution (H-3300-250, Vector). For immunofluorescence Keratin 5 (K5) staining, slides were treated with 3% H_2O_2 in PBS for 10 min and 0.1 M $NaBH_4$ in PBS for 2 h at room temperature to reduce background. After washing in 1X PBS, tissues were blocked in 1% BSA and 1% goat serum in PBS for 30 min at room temperature. Incubation with the primary antibody anti-K5 (1:1000, PRB-160P, Covance) was done overnight at 4°C. The next day, slides were washed in 1X PBS and incubated with goat anti-rabbit Dylight488 (1:1000; 35552, Thermo Fisher Scientific) and DAPI (1:1000; D1306, Life Technologies) for 30 min at room temperature. Images were acquired on a Zeiss LSM880 Fast AiryScan confocal microscope using ZEN Software (Zeiss) and processed using Fiji (ImageJ). For cleaved caspase-8 staining, slides were treated with 3% H_2O_2 in methanol for 10 minutes following the antigen retrieval step. Next, slides were washed in 1X PBS and blocking was performed using 10% goat serum in 1x PBS for 30 min. Primary antibody incubation using anti-cleaved caspase-8 (1:500; 8592S, Cell Signaling Technology) was done overnight at 4°C. Biotin goat anti-rabbit IgG (1:300; BA-1000-1.5, Vector) was used as secondary antibody. Finally, slides were incubated for 30 minutes in reagent A and B as described for the Vectastain ELITE ABC kit (PK-6100, Vector) followed

by detection with ImmPACT DAB Peroxidase (HRP) substrate kit (SK-4105, Vector). Haematoxylin counterstaining was performed using a Varistain Slide Stainer and mounted in xylene-based mounting medium. Images were acquired on a Zeiss Axio Scan slide scanner using ZEN software (Zeiss).

Cell death assays

Primary murine lung fibroblasts were seeded in 48-well plates (35,000 cells per well) or 6-well plates (330,000 cells per well) one day before treatment. HT-29 cells were seeded at 30,000 cells per well in 96-well plates. On the day of the experiment, the cell-impermeable dye SYTOX Green (1 µM, Thermo Fisher Scientific; S7020) was added to the culture medium together with the indicated stimuli. SYTOX Green uptake was imaged with an IncuCyte ZOOM Live-Cell Analysis system (Sartorius) at 37°C and 5% CO_2. The relative percentage of SYTOX Green cells was determined by dividing the number of SYTOX Green-positive cells per image by the percentage of confluency (using phase contrast images) at every time point.

Alu duplex RNA transfection

HT-29 cells were seeded in 24-well plates (130,000 cells per well) one day before transfection. The next day, medium was replaced with fresh medium containing SYTOX Green and inhibitors. Cells were transfected with 50 ng Alu duplex RNA using Lipofectamine 2000 Transfection Reagent (11668027, InvitroGen). Cell death was analysed as described before. *NICN1* and *BPNT1* 3' UTR Alu duplex RNA was kindly provided by S. Hur[39]. Alu duplex RNAs were prepared by T7 *in vitro* transcription and PAGE purification as previously described[39,52]. Alu sequences are listed in Supplementary Table 1.

Knockdown experiments

RNA silencing experiments in HT-29 cells were performed by reverse transfection using DharmaFECT 1 Transfection Reagent (T-2001, Horizon Discovery). For live-cell imaging analysis, 90,000 cells were reverse transfected at 20 nM final siRNA concentration per well of 24-well plate in medium containing the indicated stimuli or inhibitors and SYTOX Green. Cell death was analysed as described before. The following siRNAs were used in this study: ON-TARGETplus SMARTpool siRNAs (Horizon Discovery) directed against human *ADAR* (L-008630-00-0005), *ZBP1* (L-014650-00-0005), *RIPK1* (L-004445-00-0005), *RIPK3* (E-003534-00*), CASP8* (L-003466-00-0005), *TICAM1* (L-012833-00-0005), and non-targeting control (D-001810-01-05). siRNA directed against *ADAR1-p150*[53] was custom made via Thermo Fisher Scientific (Silencer Select siRNA). Sense strand: 5'-GCCUCGCGGGCGCAAUGAATT-3'; guide strand: 5'-UUCAUUGCGCCCGCGAGGCAT-3'.

Spleen, peripheral blood and skin processing for flow cytometry

Spleens of 5 day old *Adar*$^{-/-}$ *Mavs*$^{-/-}$ *Zbp1*$^{+/+,\ +/\ Z\alpha1Z\alpha2}$ or *Zbp1*$^{Z\alpha1Z\alpha2/Z\alpha1Z\alpha2}$ and control littermates were collected in ice-cold PBS. Spleens were digested for 30 min at 37°C in digestion buffer [(RPMI-1640 supplemented 0.5 mg/ml collagenase D (11088866001, Roche) and 10 mg/ml DNase I (1010459001, Roche)] with regular mixing. After neutralization with RPMI-1640 medium containing 2% FCS, erythrocytes were lysed with ACK Lysing Buffer (10-548E, Lonza) and filtered through a 70 mm cell strainer to obtain single cell solutions. Peripheral blood was collected in EDTA-coated tubes (20.1288, Sarstedt) by tail vein bleeding. 1 mL ACK Lysing Buffer (Lonza; 10-548E) was mixed with 100 ml blood and incubated for 10 min at RT. Cells were washed 2 times with ice-cold PBS and were stained for flow cytometry analysis. Pieces of shaved mouse skin (± 12 cm^2) were isolated from 21 day old *Adar*$^{+/+}$

620 *Ripk1*^{EKO} and *Adar*$^{+/Z\alpha}$ *Ripk1*^{EKO} mice or control littermates. Subcutaneous fat and muscles
621 were removed by mechanical scraping with a scalpel. Subsequently, the skin was carefully
622 placed on 0.4 mg/mL Dispase II (4492078001, Roche) with the dermal side facing downward
623 for 2h at 37°C. Epidermis was separated from the dermis with a forceps, cut into fine pieces,
624 and incubated in 2 mL enzymatic solution containing 1.5 mg/mL collagenase type IV
625 (LS004188, Worthington) and 0.5 mg/mL Dnase I (10104159001, Roche) for 20 min at 37°C
626 with shaking. After neutralization with 2% FCS RPMI medium, the cell suspension was
627 filtered through a 70 µm cell strainer to obtain a single cell suspension.
628
629 **Flow cytometry**
630 Single cell suspensions were first stained with anti-mouse CD16/CD32 (Fc block; 553142,
631 BD Biosciences) and dead cells were excluded with the Fixable Viability Dye eFluor506 (65-
632 0866-14, Thermo Fisher Scientific) for 30 min at 4°C in PBS. Next, cell surface markers were
633 stained for 30 min at 4°C in FACS buffer (PBS, 5% FCS, 1mM EDTA and 0.05% sodium
634 azide). Cells were acquired on an LSR Fortessa or a FACSymphony (BD Biosciences). Data
635 were analysed with FlowJo software (Tree Star). The total number of cells was counted on a
636 FACSVerse (BD Biosciences).
637
638 **Blood analysis**
639 Peripheral blood was collected in EDTA-coated tubes by decapitation of 5-day old pups.
640 Total number of leukocytes, erythrocytes and whole-blood parameters were determined using
641 a HEMAVET®950LV (Drew Scientific).
642
643 **Sanger sequencing**

cDNA from brain and spleen tissue derived from mice of the indicated genotypes was PCR amplified using primers targeting the mRNA of *Htr2c* (fwd: 5'-GGCCAGCACTTTCAATAGTCGTG-3', rvs: 5'-CAATCTTCATGATGGCCTTAGTCC-3'), *Mad2l1* (fwd: 5'-AATTTTCCGGTGAAGAAAGC-3', rvs: 5'-AGCTTTGATCCCTTCTGCTG-3') and *Rpa1* (fwd: 5'-CTCAGAGGGCTGTGTGTGAA-3', rvs: 5'-AGACAAAAAGGTGCCACCAC-3'). The obtained PCR product was purified with NucleoSpin® Gel and PCR Clean-up kit (740609250, Macherey-Nagel) and send for Sanger sequencing with the forward primers or in the case of *Htr2c:* 5'-GGCGAATTCCATTGCTGATATGCTGGTG-3'.

RNA-seq library preparation

Total RNA of IFNα2 treated HEK293 cells or untreated and hybrid IFNα-B/D treated primary mouse lung fibroblasts was purified using RNeasy columns (QIAGEN) with on-column DNase I digestion. RNA integrity was tested with the Agilent RNA 6000 Pico Kit (Agilent; 50671513). Sequencing libraries were prepared using the Stranded mRNA ligation kit (Illumina) with the Ribo-Zero Gold kit (Illumina) for ribosomal depletion. Deep sequencing of the libraries was performed on an Illumina Novaseq6000 generating 150 bp paired-end sequencing reads.

A-to-I editing data analysis

In order to enable a reproducible analysis from raw RNAseq data to the prediction of A-to-I editing sites by RDDpred[54], a Nextflow[55] pipeline has been developed based on the RNAseq pipeline from the nf-core community[56]. To align with our previous A-to-I data analysis[10], the original nf-core trimming module was replaced by Trimmomatic[57], the editing site prediction tool RDDpred has been inserted and a docker image has been created

669 (https://github.com/vibbits/RDDpred). For the mapping of the mouse and human samples
670 using STAR 2.7.3a, the reference genomes mm10 and hg19 have been used, respectively.
671 Positive machine learning training sets for RDDpred consisted of annotated A-to-I editing
672 sites derived from the DARNED[58], RADAR[59] and REDIportal[60] databases. The negative
673 training set consisted of Mapping Error-prone Sites observed upon mapping to the hg19 and
674 mm10 genome (http://epigenomics.snu.ac.kr/RDDpred/prior.php). The whole pipeline with
675 references to the genome and STAR indices is available on github
676 https://github.com/vibbits/rnaseq-editing. This pre-processing pipeline has been executed on
677 the human and mice samples using the Azure Kubernetes Services. The raw output of
678 RDDpred was further analysed by assigning strand topology to each identified RNA-DNA
679 difference (RDD). To this end, BAM files were split in half-samples containing reads that
680 were either mapped to the sense or antisense strand. Next, quantification of total read
681 coverage and variant read frequency was performed for all detected A>G and T>C RDDs in
682 each half-sample using Bam-readcount (https://github.com/genome/bam-readcount).
683 Ambiguous RDDs (e.g., multiple variant calls per site, RDDs detected on both strands),
684 RDDs (murine dataset) overlapping with annotated C57BL/6-specific SNPs (Sanger Institute
685 Mouse Genomes project v3; dbSNPv137) or (human dataset) HEK293-specific SNPs
686 (http://hek293genome.org/v2/data.php; data trackCG293, converted to hg19 assembly using
687 LiftOver) and RDDs that were also detected in ADAR1-deficient cells were removed from the
688 datasets. Finally, identified editing sites with a read coverage below 10 or that were observed
689 in less than 3 different samples (independent of genotype) were excluded from the final
690 datasets. Next, repeat element status of each editing site was determined based on the
691 RepeatMasker annotation (www.repeatmasker.org; Repeat Library 20140131) and repeat/Alu
692 editing index was calculated by dividing the combined number of detected variants (A>G or
693 T>C) by the combined total number of reads covering the A-to-I editing sites identified in a

single repeat element. Repeat/Alu elements of which editing activity was restricted to a single genotype were reported when editing was observed in all samples of that genotype. For differential editing analysis, only repeat/Alu elements that displayed editing in all three wild type and all three mutant samples were included. Differentially edited repeats/Alu elements (p value < 0.05) were determined by Welch Two Sample t test on the log10 values of the calculated editing index. See Supplementary Table 2 for a list of differentially edited repeat/Alu elements. *In silico* RNA folding analysis was performed using the RNAfold webtool from the Vienna RNA Websuite[61] using the default parameters and the algorithm 'minimum free energy (MFE) and partition function'. The change in folding characteristics due to A-to-I editing was calculated by introducing constraints that mimic complete lack of base pairing on the identified A-to-I editing sites.

Statistical analysis

Statistical analyses were performed in Prism 8.3.0 (GraphPad Software). Statistical methods are described in the figure legends.

Data availability

Raw RNA sequencing data used in this study is available on the European Nucleotide Archive (https://www.ebi.ac.uk/ena/browser/home), accession codes PRJEB52610 (mouse primary lung fibroblasts) and PRJEB52618 (HEK293 cells). Source data belonging to Figures 1-4 and Extended Data Figures 1-10 are provided with the paper.

Code availability

The complete pipeline used for the A-to-I editing analysis from raw RNAseq data to the original output of the editing site prediction tool RDDpred with references to the genome and

719 STAR indices is made available on github (https://github.com/vibbits/rnaseq-editing). Any
720 additional information required to reanalyse the data reported in this paper is available from
721 the lead contact upon request.
722

Methods references

39 Ahmad, S. *et al.* Breaching Self-Tolerance to Alu Duplex RNA Underlies MDA5-Mediated Inflammation. *Cell* **172**, 797-810 e713, doi:10.1016/j.cell.2017.12.016 (2018).

45 Michallet, M. C. *et al.* TRADD protein is an essential component of the RIG-like helicase antiviral pathway. *Immunity* **28**, 651-661, doi:10.1016/j.immuni.2008.03.013 (2008).

46 Newton, K., Sun, X. & Dixit, V. M. Kinase RIP3 is dispensable for normal NF-kappa Bs, signaling by the B-cell and T-cell receptors, tumor necrosis factor receptor 1, and Toll-like receptors 2 and 4. *Mol Cell Biol* **24**, 1464-1469, doi:10.1128/MCB.24.4.1464-1469.2004 (2004).

47 Hayashi, S., Lewis, P., Pevny, L. & McMahon, A. P. Efficient gene modulation in mouse epiblast using a Sox2Cre transgenic mouse strain. *Mech Dev* **119 Suppl 1**, S97-S101, doi:10.1016/s0925-4773(03)00099-6 (2002).

48 Murphy, J. M. *et al.* The pseudokinase MLKL mediates necroptosis via a molecular switch mechanism. *Immunity* **39**, 443-453, doi:10.1016/j.immuni.2013.06.018 (2013).

49 Beisner, D. R., Ch'en, I. L., Kolla, R. V., Hoffmann, A. & Hedrick, S. M. Cutting edge: innate immunity conferred by B cells is regulated by caspase-8. *J Immunol* **175**, 3469-3473, doi:10.4049/jimmunol.175.6.3469 (2005).

50 Huang, Z. *et al.* RIP1/RIP3 binding to HSV-1 ICP6 initiates necroptosis to restrict virus propagation in mice. *Cell Host Microbe* **17**, 229-242, doi:10.1016/j.chom.2015.01.002 (2015).

51 De Groote, P. *et al.* Generation of a new Gateway-compatible inducible lentiviral vector platform allowing easy derivation of co-transduced cells. *Biotechniques* **60**, 252-259, doi:10.2144/000114417 (2016).

52 Peisley, A. *et al.* Cooperative assembly and dynamic disassembly of MDA5 filaments for viral dsRNA recognition. *Proc Natl Acad Sci U S A* **108**, 21010-21015, doi:10.1073/pnas.1113651108 (2011).

53 Sakurai, M. *et al.* ADAR1 controls apoptosis of stressed cells by inhibiting Staufen1-mediated mRNA decay. *Nat Struct Mol Biol* **24**, 534-543, doi:10.1038/nsmb.3403 (2017).

54 Kim, M. S., Hur, B. & Kim, S. RDDpred: a condition-specific RNA-editing prediction model from RNA-seq data. *BMC Genomics* **17 Suppl 1**, 5, doi:10.1186/s12864-015-2301-y (2016).

55 Di Tommaso, P. *et al.* Nextflow enables reproducible computational workflows. *Nat Biotechnol* **35**, 316-319, doi:10.1038/nbt.3820 (2017).

56 Ewels, P. A. *et al.* The nf-core framework for community-curated bioinformatics pipelines. *Nat Biotechnol* **38**, 276-278, doi:10.1038/s41587-020-0439-x (2020).

57 Bolger, A. M., Lohse, M. & Usadel, B. Trimmomatic: a flexible trimmer for Illumina sequence data. *Bioinformatics* **30**, 2114-2120, doi:10.1093/bioinformatics/btu170 (2014).

58 Kiran, A. M., O'Mahony, J. J., Sanjeev, K. & Baranov, P. V. Darned in 2013: inclusion of model organisms and linking with Wikipedia. *Nucleic Acids Res* **41**, D258-261, doi:10.1093/nar/gks961 (2013).

59 Ramaswami, G. & Li, J. B. RADAR: a rigorously annotated database of A-to-I RNA editing. *Nucleic Acids Res* **42**, D109-113, doi:10.1093/nar/gkt996 (2014).

60 Mansi, L. *et al.* REDIportal: millions of novel A-to-I RNA editing events from thousands of RNAseq experiments. *Nucleic Acids Res* **49**, D1012-D1019, doi:10.1093/nar/gkaa916 (2021).
61 Lorenz, R. *et al.* ViennaRNA Package 2.0. *Algorithms Mol Biol* **6**, 26, doi:10.1186/1748-7188-6-26 (2011).

Acknowledgements. We are grateful to the VIB-UGent IRC Animal house for mouse husbandry. We would like to thank the VIB Flow and Bioimaging Cores for training, support and access to the instrument park. Research in the J.M. group was supported by an Odysseus II Grant (G0H8618N), EOS INFLADIS (40007512), a junior research grant (G031022N) from the Research Foundation Flanders (FWO), a CRIG young investigator proof-of-concept grant and by Ghent University. Research in the P.V. group was supported by EOS MODEL-IDI (30826052), EOS INFLADIS (40007512), FWO senior research grants (G.0C76.18N, G.0B71.18N, G.0B96.20N, G.0A9322N), Methusalem (BOF16/MET_V/007), iBOF20/IBF/039 ATLANTIS, Foundation against Cancer (F/2016/865, F/2020/1505), CRIG and GIGG consortia, and VIB. Research in the S.H. group was supported by NIH grants R01AI154653 and R01AI111784. R.d.R. was supported by a Ghent University BOF PhD fellowship. S.V and J.N. were supported by FWO PhD fellowships.

Author contributions. R.d.R., S.V. and J.M. conceived the study. R.d.R., S.V., E.D., J.N., and J.M. designed, performed and analysed experiments and interpreted data. E.H., M.J. and G.B. performed and analysed experiments, F.V.N., L.V. G.v.L. and W.D, helped with experimental design, A.B. performed bioinformatical analysis, S.A. and S.H. generated Alu:Alu hybrids, J.M. supervised the experiments. R.d.R., S.V., P.V. and J.M. wrote the manuscript.

Competing interests. The authors declare no competing interests.

Correspondence and requests for materials should be addressed to J.M.

Extended Data Figures

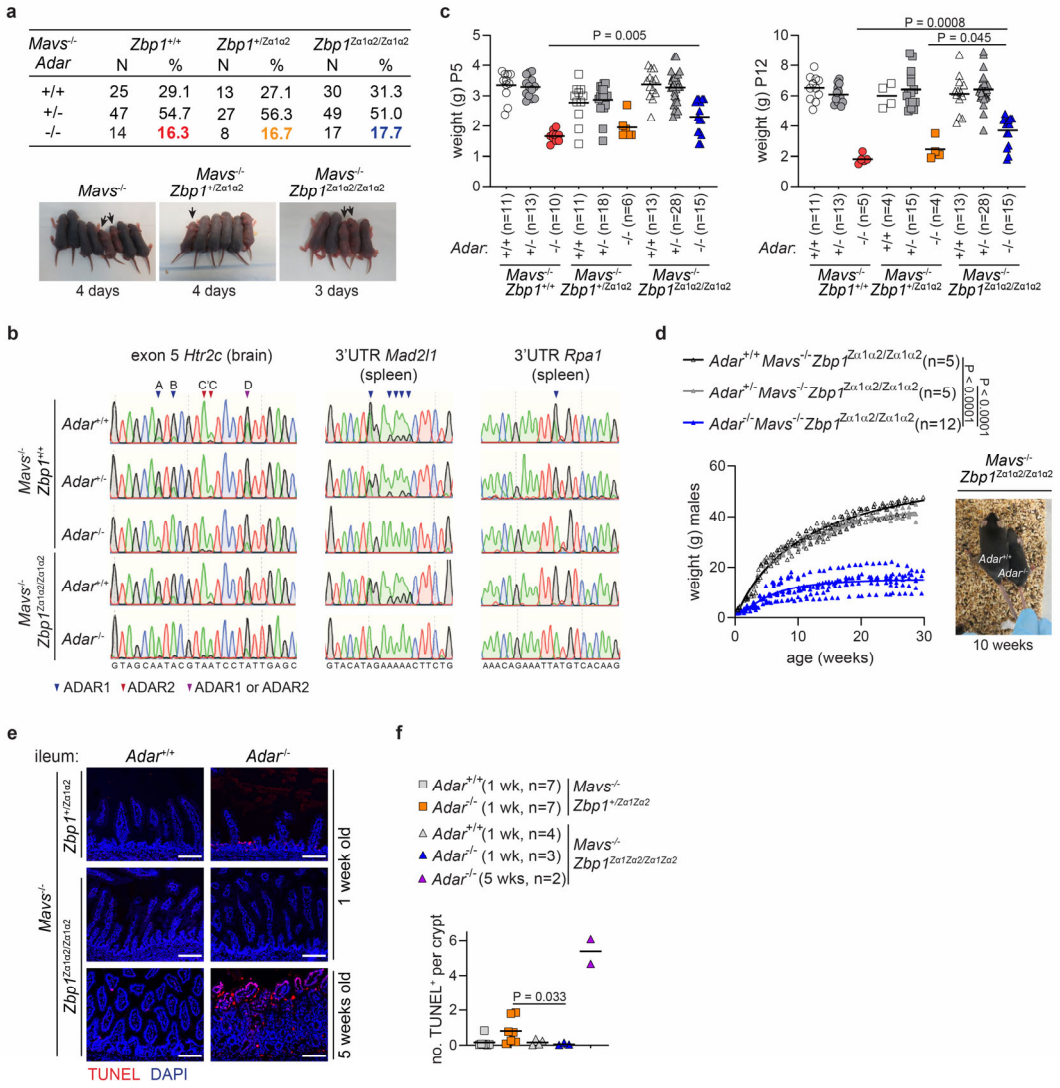

Extended Data Fig. 1. Characterisation of *Adar*$^{-/-}$ *Mavs*$^{-/-}$ *Zbp1*$^{Zα1α2/Zα1α2}$ mice. a, Numbers and percentages of pups obtained from *Adar*$^{+/-}$ *Mavs*$^{-/-}$ *Zbp1*$^{+/+, +/Zα1α2 \text{ or } Zα1α2/Zα1α2}$ breeding pairs. Lower panels show representative images of 3 or 4 day old pups. Arrows indicate *Adar/Mavs* double knockout mice with the indicated *Zbp1* genotypes. **b,** Sanger sequencing chromatograms of A-to-I editing sites in brain (*Htr2c*) or spleen (*Mad2l1* and *Rpa1*) tissues derived from mice of the indicated genotypes. ADAR1-, ADAR2- and ADAR1/ADAR2-specific sites indicated by blue, red and purple triangles, respectively. **c,** Weight in grams (g) of 5 (P5) or 12 (P12) day old mice of the indicated genotypes. **d,** Weight in grams (g) of male

mice of the indicated genotypes measured weekly from birth till 30 weeks of age. Right panel shows a representative picture of a 10 week old *Adar*$^{-/-}$ *Mavs*$^{-/-}$ *Zbp1*$^{Zα1α2/Zα1α2}$ mouse and an *Adar*$^{+/+}$ *Mavs*$^{-/-}$ *Zbp1*$^{Zα1α2/Zα1α2}$ littermate. **e,** TUNEL assay on ileum sections from 1 week or 5 week old *Adar*$^{-/-}$ *Mavs*$^{-/-}$ mice expressing Zα domain mutant ZBP1 from one (*Zbp1*$^{+/Zα1α2}$) or two (*Zbp1*$^{Zα1α2/Zα1α2}$) alleles. Scale bar = 100 μm. **f,** quantification of TUNEL^{+} cells per crypt. Each data point in **(c,d,f)** represents an individual mouse. The numbers of mice (n) that were analysed per genotype in **(c,d,f)** are indicated in the graph. Lines in **(c,f)** represent the mean; P values by Mann-Whitney test. Lines in **(d)** represent a sigmoidal, 4PL fit; P values by two-way ANOVA.

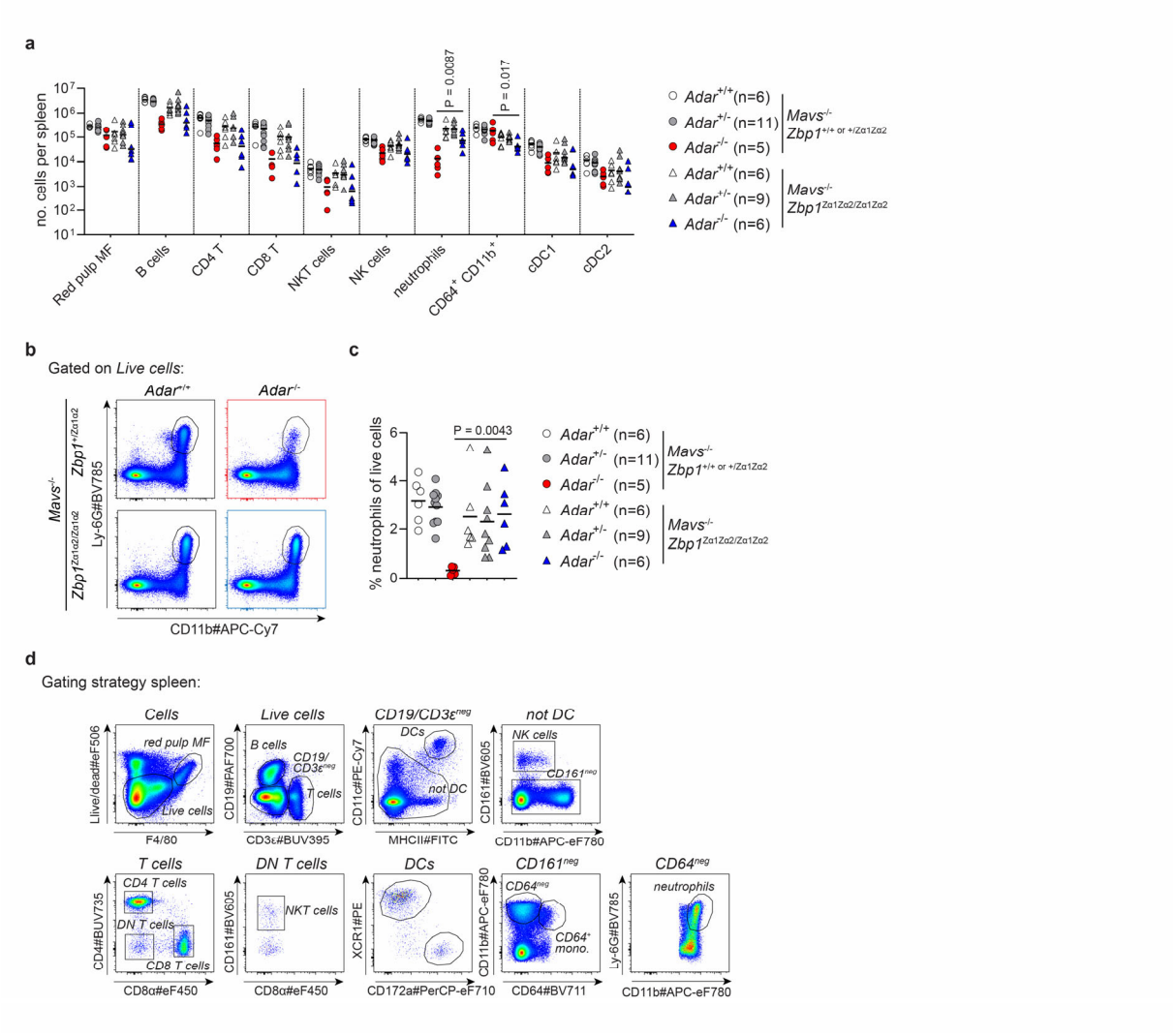

821

822 **Extended Data Fig. 2. Immune phenotyping of *Adar*$^{-/-}$ *Mavs*$^{-/-}$ *Zbp1*$^{Zα1α2/\ Zα1α2}$ mice. a,**
823 Flow cytometric quantification of numbers of immune cell populations in spleens of 4 to 5
824 day old *Adar*$^{-/-}$ *Mavs*$^{-/-}$ mice expressing wild-type (*Zbp1*$^{+/+,\ +/Zα1Zα2}$) or Zα domain mutant
825 ZBP1 (*Zbp1*$^{Zα1α2/Zα1α2}$). **b,** Representative flow plots showing the presence of neutrophils in
826 live cell populations in spleens of mice of the indicated genotypes. **c,** Percentage of
827 neutrophils in the population of live cells in spleens. **d,** Flow cytometry gating strategy of
828 immune cell populations in spleens shown in **(a,b)**. Lines in **(a,c)** represent the mean; each
829 data point represents an individual mouse; the numbers of mice (n) that were analysed per
830 genotype are indicated in the graph; P values by Mann-Whitney test.

831

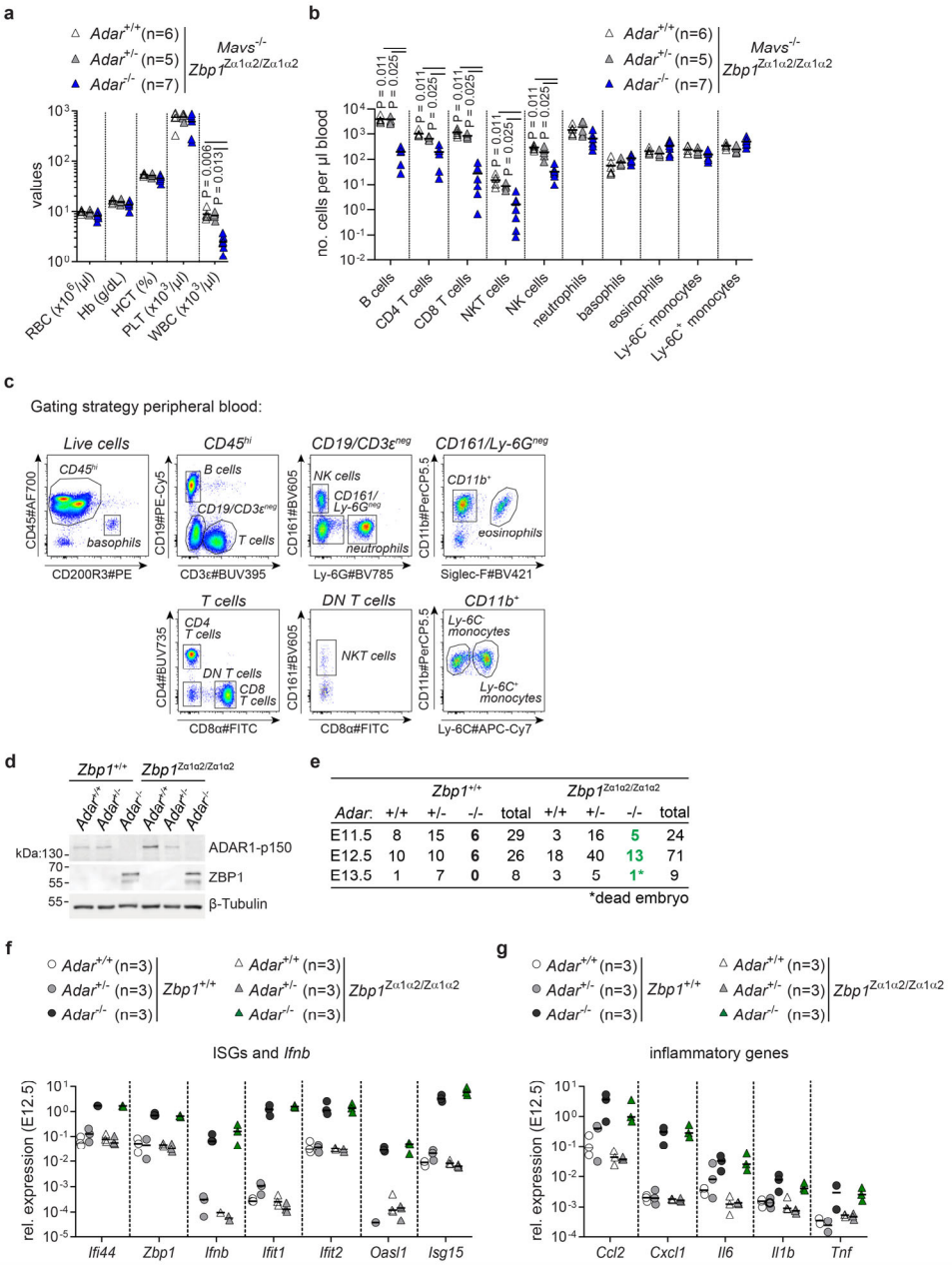

Adar:	Zbp1+/+ +/+	+/-	-/-	total	Zbp1Zα1α2/Zα1α2 +/+	+/-	-/-	total
E11.5	8	15	6	29	3	16	5	24
E12.5	10	10	6	26	18	40	13	71
E13.5	1	7	0	8	3	5	1*	9

*dead embryo

Extended Data Fig. 3. Immune phenotyping of surviving *Adar*$^{-/-}$ *Mavs*$^{-/-}$ *Zbp1*$^{Zα1α2/Zα1α2}$ mice and analysis of *Adar*$^{-/-}$ *Zbp1*$^{Zα1α2/Zα1α2}$ embryos. a, Peripheral blood of 20 week old *Adar*$^{-/-}$ *Mavs*$^{-/-}$ *Zbp1*$^{Zα1α2/Zα1α2}$ pups and their littermates was analysed for total red blood cell (RBC), white blood cell (WBC) and platelet (PLT) numbers, together with haemoglobin (Hb) and haematocrit (HCT) levels. **b,** Flow cytometric quantification of numbers of circulating lymphocytes (B cells, CD4 and CD8 T cells, and NK and NKT cells) or myeloid cells (neutrophils, basophils, eosinophils and Ly-6C^{-} and Ly-6C^{+} monocytes) per µL of blood. **c,**

840 Gating strategy for flow cytometry analysis in **(b)**. **d,** Immunoblot analysis of embryonic (E)
841 day 12.5 whole embryo lysates of the indicated genotypes. **e**, Numbers of embryos resulting
842 from interbreeding of *Adar*$^{+/-}$ *Zbp1*$^{+/+ \text{ or } Z\alpha1\alpha2/Z\alpha1\alpha2}$ breeding pairs and dissected on the indicated
843 embryonic (E) days. **f,g,** RT-qPCR analysis of the indicated ISGs and *Ifnb* **(f)** or inflammatory
844 genes **(g)** analysed in E12.5 embryos of the indicated genotypes. Lines in (**a**,**b**,**f,g**) represent
845 the mean; each data point represents an individual mouse; each data point represents an
846 individual mouse; the numbers of mice (n) that were analysed per genotype are indicated in
847 the graph; P values by Mann-Whitney test. For gel source data, see Supplementary Figure 1.
848
849

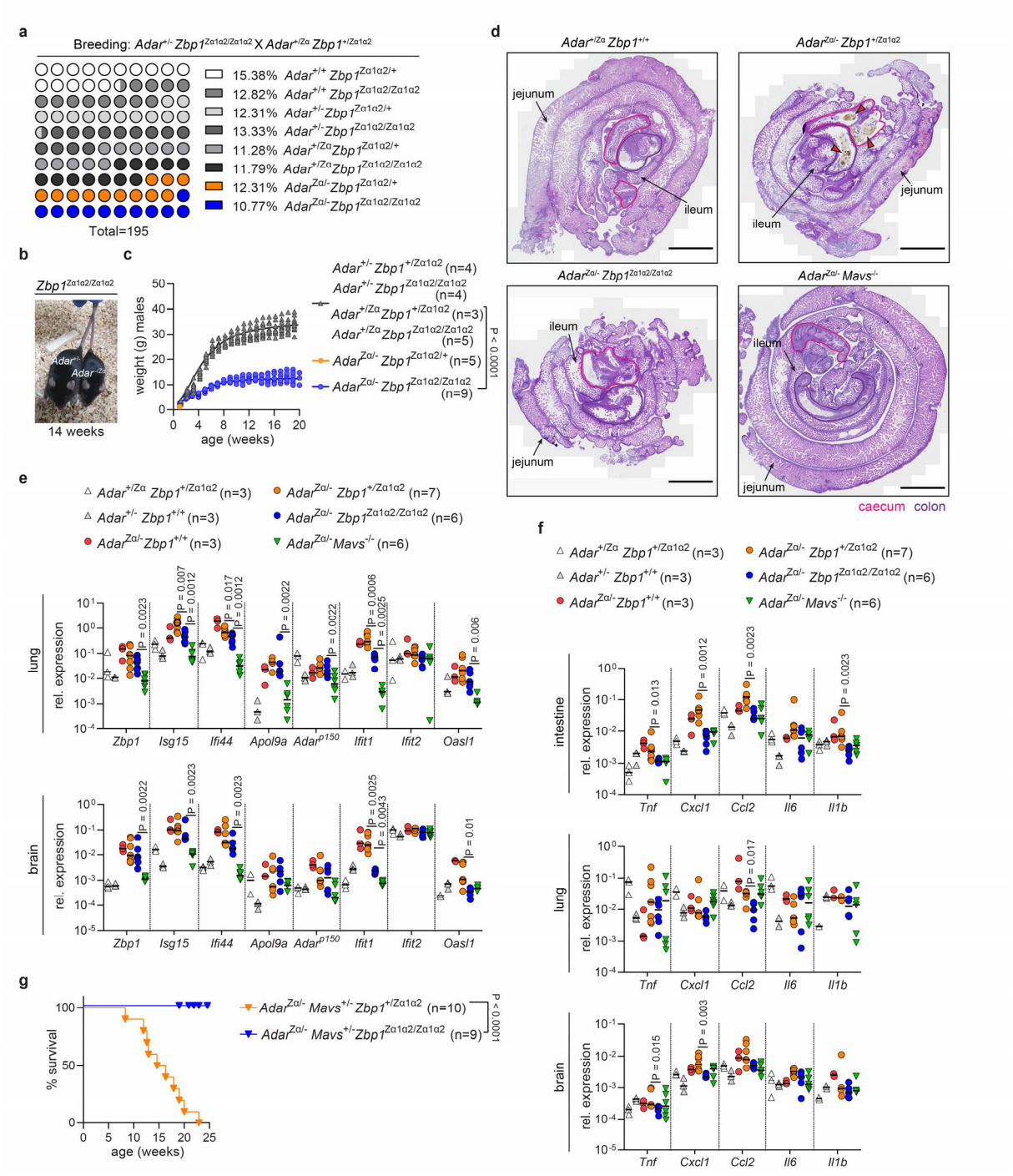

Extended Data Fig. 4. Characterisation of *Adar*$^{Zα/-}$ *Zbp1*$^{Zα1α2/Zα1α2}$ and *Adar*$^{Zα/-}$ *Mavs*$^{+/-}$ *Zbp1*$^{Zα1α2/Zα1α2}$ mice. a, Percentages of offspring (n=195) with the indicated genotypes obtained from *Adar*$^{+/-}$ *Zbp1*$^{Zα1α2/Zα1α2}$ X *Adar*$^{+/Zα}$ *Zbp1*$^{+/Zα1α2}$ breeding pairs. **b,** Representative image of a 14 week old *Adar*$^{Zα/-}$ *Zbp1*$^{Zα1α2/Zα1α2}$ mouse and its *Adar*$^{+/-}$ *Zbp1*$^{Zα1α2/Zα1α2}$ littermate. **c,** Weight in grams (g) of male mice of the indicated genotypes measured weekly from birth

856 till 20 weeks of age. Each data point represents an individual mouse; lines represent a
857 sigmoidal, 4PL fit; P value by two-way ANOVA. **d,** H&E staining of longitudinal sections of
858 whole intestines from 1 day old mice from the indicated genotypes. Jejunum and ileum are
859 indicated by arrows. Caecum and colon are indicated by a pink and purple line, respectively.
860 Scale bar = 0.2 cm. Red triangles indicate necrotic tissue in caecum and colon. **e,** RT-qPCR
861 analysis of the indicated ISGs, analysed in whole tissue lysates of lungs and brains of 1 day
862 old pups of the indicated genotypes. **f,** RT-qPCR analysis of the indicated inflammatory
863 genes, analysed in whole tissue lysates of intestines, lungs and brains of 1 day old pups of the
864 indicated genotypes. Lines in **(e, f)** represent the mean; each data point represents an
865 individual mouse; P values by Mann-Whitney test. **g,** Kaplan-Meier survival curve of mice
866 from the indicated genotypes. P value by log-rank test. Numbers of mice (n) that were
867 analysed per genotype in **(c,e,f,g)** are indicated in the graph.
868
869

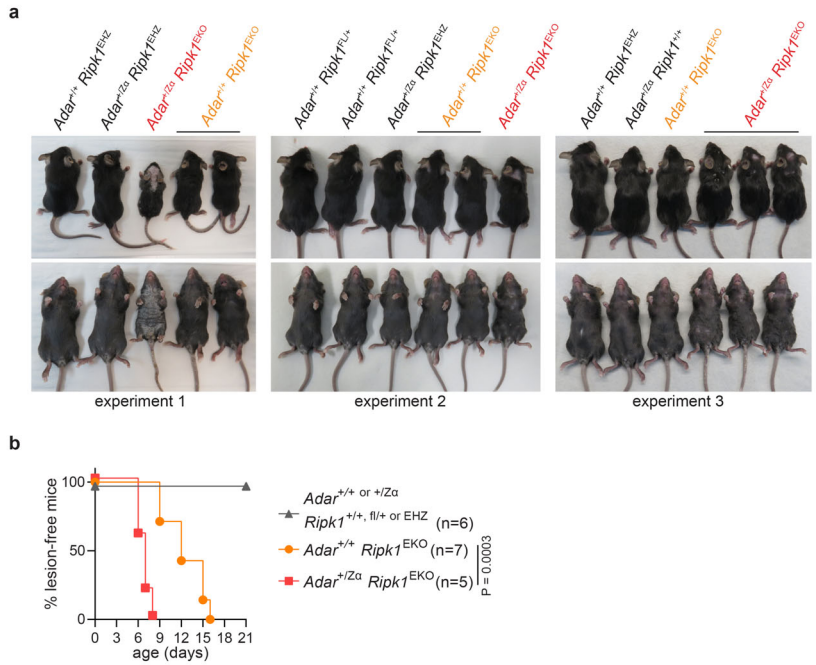

870

871 **Extended Data Fig. 5. *Adar*$^{+/Zα}$ *Ripk1*^{EKO} mice develop severe skin inflammation. a,**
872 Macroscopic images of 21 day old *Adar*$^{+/+}$ *Ripk1*^{EKO} mice, *Adar*$^{+/Zα}$ *Ripk1*^{EKO} mice and control
873 littermates from 3 experiments. **b,** Kaplan-Meier plot of macroscopically visible lesion
874 appearance of epidermis-specific RIPK1 knockout mice (*Ripk1*^{EKO}) carrying heterozygous
875 ADAR1 Zα domain mutant alleles (*Adar*$^{+/Zα}$) or expressing wild type ADAR1. Littermate
876 offspring containing two or one wild type *Ripk1* alleles (*Ripk1*$^{+/+,\ fl/+}$) or heterozygously
877 expressing a functional *Ripk1* allele in the epidermis (*Ripk1*^{EHZ}) did not develop lesions and
878 are shown as controls. Numbers of mice (n) that were analysed per genotype are indicated in
879 the graph. P value by log-rank test.

880

881

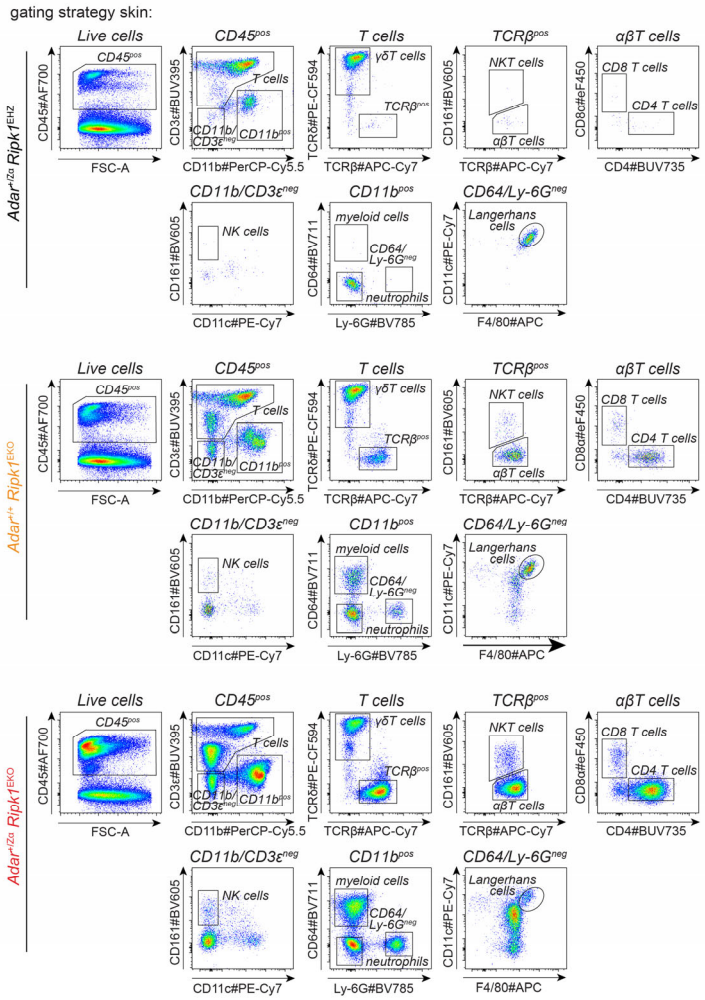

882

883 **Extended Data Fig. 6. Flow cytometry gating strategy of CD45$^+$ immune cell subsets in**

884 **the skin**. Representative flow plots of the immune cell subsets of the indicated genotypes are

885 shown. The data are shown quantified in Fig. 2g.

886

887

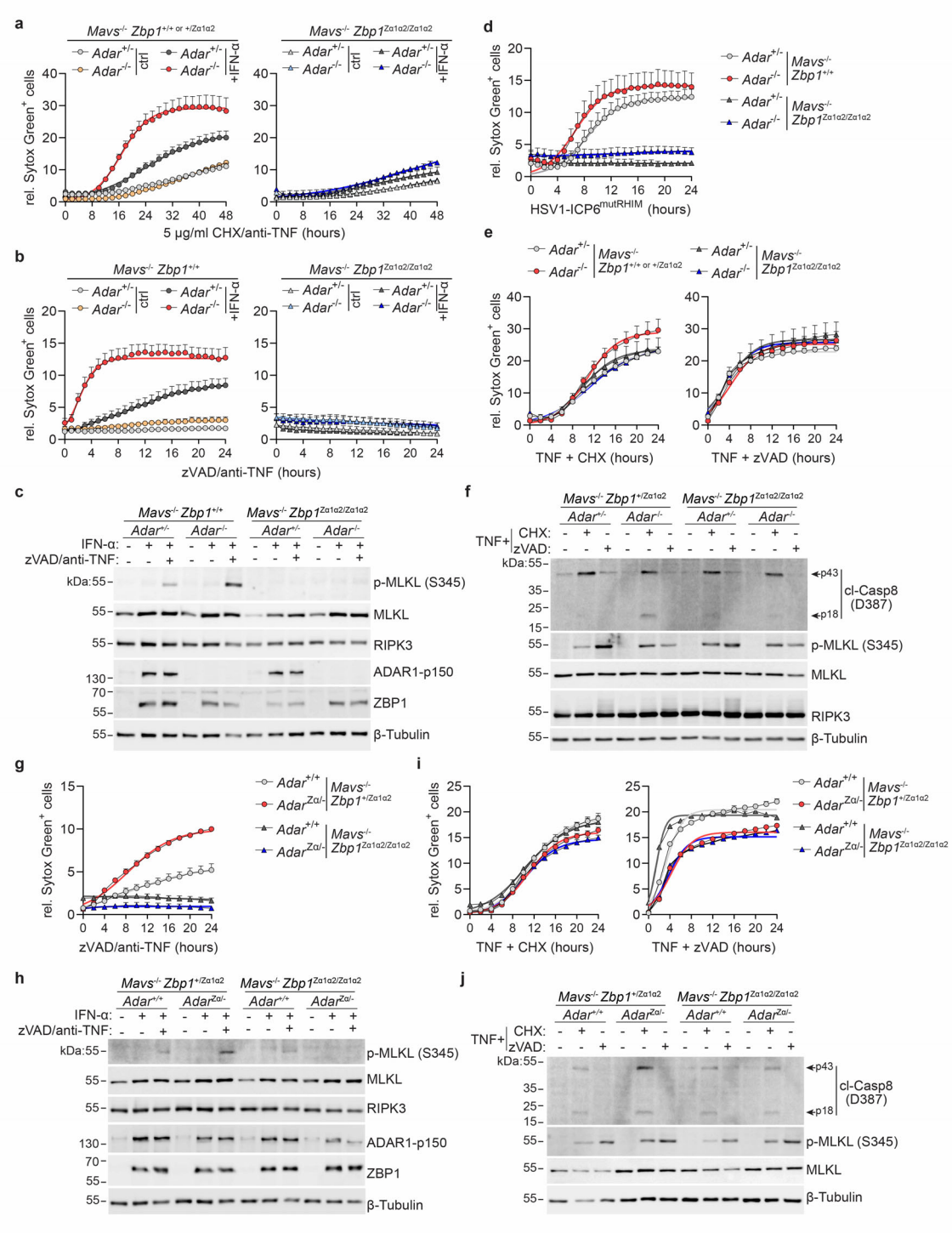

888

889 **Extended Data Fig. 7. ADAR1 deletion or Zα domain mutation induces ZBP1-mediated**
890 **cell death of mouse fibroblasts. a-j,** Primary mouse lung fibroblasts isolated from mice of
891 the indicated genotypes were stimulated with 200 U/mL IFN-α **(a-c, e-j)** or 200 U/mL IFN-γ
892 **(d)** for 16 hours or left untreated (ctrl). Next, cells were treated with 5 μg/mL CHX and 1
893 μg/mL anti-mouse TNF **(a)**, 50 μM zVAD-fmk and 1 μg/mL anti-mouse TNF **(b,c,g,h)**, 30

894 ng/mL mouse TNF and 10 μg/mL CHX or 50 μM zVAD-fmk **(e,f,i,j)** or infected with HSV1
895 ICP6^{mutRHIM} at a multiplicity of infection of 5 **(d)**. Cell death in **(a,b,d,e,g,i)** was quantified by
896 measuring relative (rel.) SYTOX Green uptake every 2 hours. **c,** Immunoblot related to **(b)**.
897 Samples were harvested 4 hours post treatment. **f,j** Immunoblot related to **(e,i)**. Samples were
898 harvested 7 (TNF + CHX) and 3 (TNF + zVAD) hours, respectively. **h,** Immunoblot related to
899 **(g)**. Samples were harvested 8 hours post treatment. Data points in **(a,b,d,e,g,i)** show the
900 mean of 2-6 technical replicates (see Source Data) + SD and are representative of 3
901 independent experiments. Fitted lines represent a logistic growth fit. For gel source data, see
902 Supplementary Figure 1.
903
904

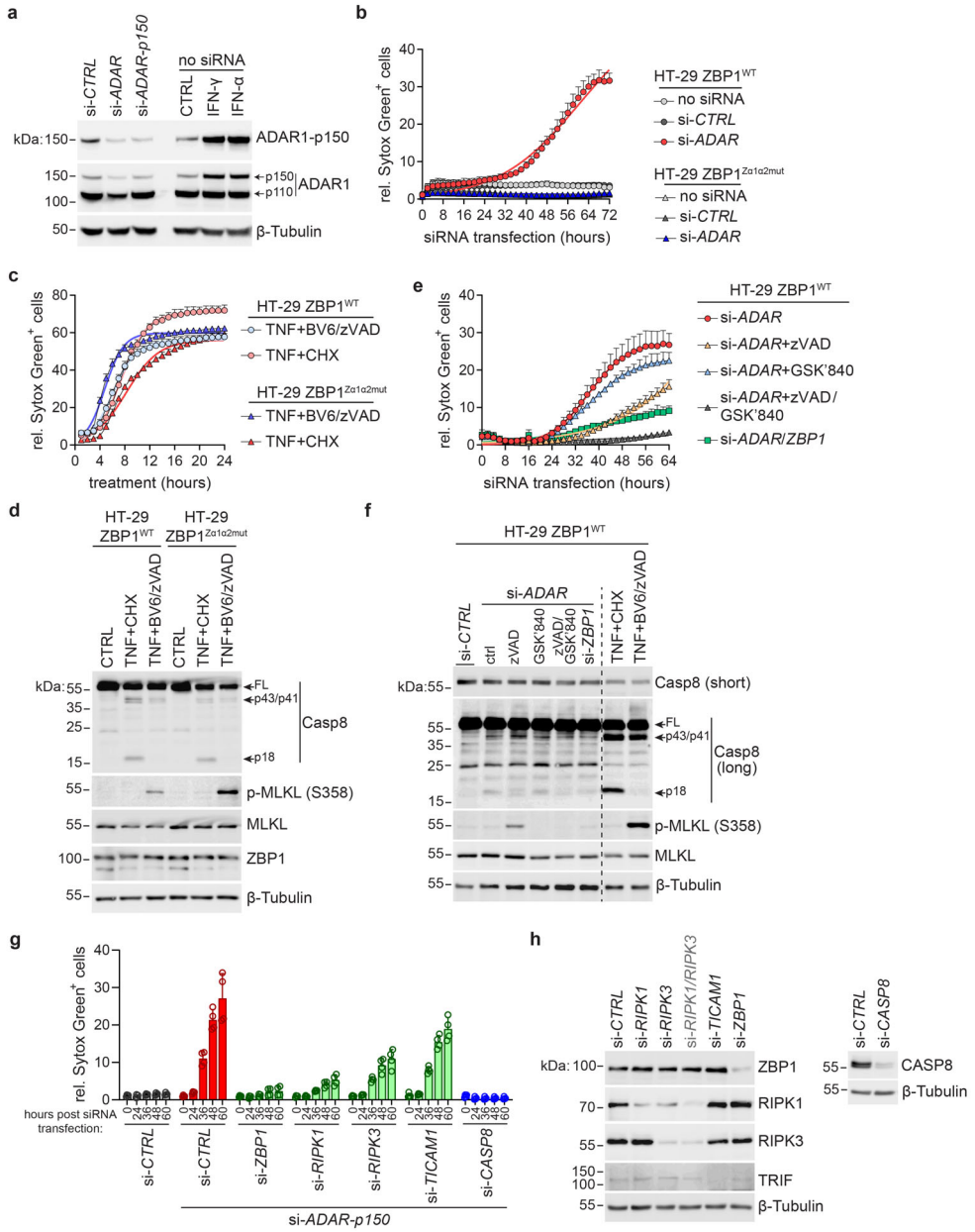

Extended Data Figure 8. ADAR1 depletion causes ZBP1-dependent cell death of human HT-29 cells. a, Immunoblot of HT-29 cells 48 hours post transfection with non-targeting control siRNAs (si-*CTRL*), siRNAs targeting *ADAR* (si-*ADAR*) or the p150 isoform of *ADAR* (si-*ADAR-p150*). As controls, cells were treated with 1,000 U/mL IFN-α or 100 ng/mL IFN-γ. **b,** HT-29 cells stably expressing wild type ZBP1 (ZBP1^{WT}) or Zα domain mutant ZBP1 (ZBP1^{Zα1Zα2mut}) were transfected with non-targeting control siRNAs (si-*CTRL*) or siRNAs targeting *ADAR* (si-*ADAR*). Cell death was quantified by measuring relative (rel.) SYTOX

Green uptake every 2 hours. **c,** HT-29 ZBP1^{WT} and ZBP1^{Zα1Zα2mut} cells were treated with 30 ng/mL human TNF, 5 μM BV6 and 20 μM zVAD-fmk (TNF + BV6/ZVAD) or 30 ng/mL TNF and 20 μg/mL CHX (TNF + CHX). Cell death was quantified as in **(b)**. **d,** Immunoblot related to **(c)**. Cells were harvested 3 (TNF + BV6/ZVAD) or 6 (TNF+CHX) hours post treatment. **e,** HT-29 ZBP1^{WT} cells were transfected with si-*ADAR* only or si-*ADAR* and si-*ZBP1*. After five hours, cells were treated with 20 μM zVAD-fmk and/or 3 μM GSK'840 or left untreated. Cell death was analysed as in **(b)**. **f,** Immunoblot related to **(e)**. Samples were harvested 30 hours post transfection. TNF + CHX and TNF + BV6/ZVAD control samples were treated and harvested as in **(d)**. **g,** HT-29 ZBP1^{WT} cells were transfected with si-*CTRL* or si-*ADAR-p150*. si-*ADAR-p150* was combined with si-*ZBP1*, or siRNAs targeting *RIPK1* (si-*RIPK1*), *RIPK3* (si-*RIPK3*), *TICAM1* (TRIF; si-*TICAM1*) or *CASP8* (si-*CASP8*). Cell death was quantified as in **(b)**. **h,** HT-29 ZBP1^{WT} cells transfected with the indicated siRNAs were harvested at 48 hours post transfection for protein expression analysis. Fitted lines in **(b,c,e)** represent a logistic growth fit; Data points show mean of 3 **(b,c,e)** or 4 **(g)** technical replicates + SD and are representative of 3 independent experiments. For gel source data, see Supplementary Figure 1.

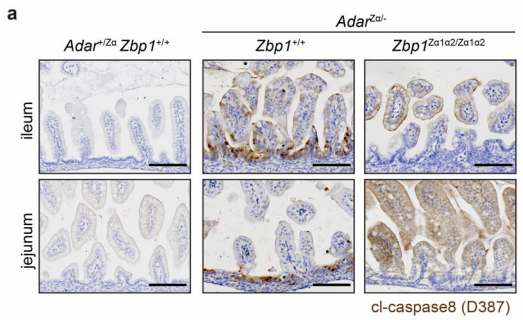

d

Breeding: *Adar*$^{+/-}$ *Mlkl*$^{-/-}$ X *Adar*$^{+/Zα}$ *Mlkl*$^{-/-}$

Adar	*Mlkl*	n	obs.%	exp.%
+/+	-/-	9	26.5	25.0
+/-	-/-	10	29.4	25.0
+/Zα	-/-	9	26.5	25.0
Zα/-	-/-	6	17.7	25.0

e

Breeding: *Adar*$^{+/-}$ *Mlkl*$^{-/-}$ X *Adar*$^{Zα/Zα}$ *Mlkl*$^{-/-}$

	Mlkl	n	obs.%	exp.%
+/Zα	-/-	31	57.4	50.0
Zα/-	-/-	23	42.6	50.0

b

Breeding: *Adar*$^{+/-}$ *Ripk3*$^{+/-}$ X *Adar*$^{+/Zα}$ *Ripk3*$^{+/-}$

Adar	*Ripk3*	n	obs.%	exp.%
+/+	+/+	13	6.25	6.25
+/+	+/-	27	13.0	12.5
+/+	-/-	27	8.17	6.25
+/-	+/+	11	5.29	6.25
+/-	+/-	37	17.8	12.5
+/-	-/-	12	5.77	6.25
+/Zα	+/+	18	8.65	6.25
+/Zα	+/-	25	12.02	12.5
+/Zα	-/-	8	3.85	6.25
Zα/-	+/+	12	5.77	6.25
Zα/-	+/-	19	9.13	12.5
Zα/-	-/-	9	4.33	6.25

f

Breeding: *Adar*$^{+/-}$ *Mlkl*$^{-/-}$ *Casp8*$^{+/-}$ X *Adar*$^{+/Zα}$ *Mlkl*$^{-/-}$ *Casp8*$^{+/-}$

Adar	*Mlkl*	*Casp8*	n	obs.%	exp.%
+/+	-/-	+/+	5	7.46	6.25
+/+	-/-	+/-	9	13.4	12.5
+/+	-/-	-/-	4	5.97	6.25
+/-	-/-	+/+	5	7.46	6.25
+/-	-/-	+/-	8	12.0	12.5
+/-	-/-	-/-	9	13.4	6.25
+/Zα	-/-	+/+	3	4.48	6.25
+/Zα	-/-	+/-	12	18.0	12.5
+/Zα	-/-	-/-	4	5.97	6.25
Zα/-	-/-	+/+	0	0.00	6.25
Zα/-	-/-	+/-	7	10.5	12.5
Zα/-	-/-	-/-	1	1.49	6.25

c

	Adar$^{Zα/-}$		
Ripk3:	+/+	+/-	-/-
≤ P2	8	10	8
> P2	0	2*	1#

**died at P3 and # at P6*

g

Breeding: *Adar*$^{+/-}$ *Mlkl*$^{-/-}$ *Casp8*$^{+/-}$ X *Adar*$^{Zα/Zα}$ *Mlkl*$^{-/-}$ *Casp8*$^{+/-}$

Adar	*Mlkl*	*Casp8*	n	obs.%	exp.%
+/Zα	-/-	+/+	6	7.59	12.5
+/Zα	-/-	+/-	26	33.0	25.0
+/Zα	-/-	-/-	10	12.7	12.5
Zα/-	-/-	+/+	5	6.33	12.5
Zα/-	-/-	+/-	27	34.2	25.0
Zα/-	-/-	-/-	5	6.33	12.5

h

	Adar$^{Zα/-}$ *Mlkl*$^{-/-}$		
Casp8:	+/+	+/-	-/-
≤ P2	19	17	3
> P2	0	0	0

Extended Data Fig. 9. Characterisation of *Adar*$^{Zα/-}$ *Ripk3*$^{-/-}$ and *Adar*$^{Zα/-}$ *Mlkl*$^{-/-}$ *Casp8*$^{-/-}$ mice. a, Sections from ileum or jejunum of *Adar*$^{+/Zα}$ *Zbp1*$^{+/+}$ and *Adar*$^{Zα/-}$ *Zbp1*$^{+/+}$ or *Zbp1*$^{Zα1Zα2/Zα1Zα2}$ mice stained for cleaved caspase-8 (D387) and counterstained with haematoxylin. Scale bars = 100 µm. At least 3 mice per genotype were analysed. **b,** Numbers (n) and percentages of pups obtained from interbreeding of *Adar*$^{+/-}$ *Ripk3*$^{+/-}$ X *Adar*$^{+/Zα}$ *Ripk3*$^{+/-}$ mice. **c,** Number of *Adar*$^{Zα/-}$ *Ripk3*$^{+/+}$, *Adar*$^{Zα/-}$ *Ripk3*$^{+/-}$ or *Adar*$^{Zα/-}$ *Ripk3*$^{-/-}$ that survived beyond day 2 after birth (> P2). **d,** Numbers and percentages of pups obtained from interbreeding of *Adar*$^{+/-}$ *Mlkl*$^{-/-}$ X *Adar*$^{+/Zα}$ *Mlkl*$^{-/-}$ mice. **e,** Numbers and percentages of pups obtained from interbreeding of *Adar*$^{+/-}$ *Mlkl*$^{-/-}$ X *Adar* $^{Zα/Zα}$ *Mlkl*$^{-/-}$ mice. **f,** Numbers and percentages of pups obtained from interbreeding of *Adar*$^{+/-}$ *Mlkl*$^{-/-}$ *Casp8*$^{+/-}$ X *Adar*$^{+/Zα}$ *Mlkl*$^{-/-}$

Casp8$^{+/-}$ mice. **g,** Numbers and percentages of pups obtained from interbreeding of *Adar*$^{+/-}$ *Mlkl*$^{-/-}$ *Casp8*$^{+/-}$ X *Adar* $^{Zα/Zα}$ *Mlkl*$^{-/-}$ *Casp8*$^{+/-}$ mice. **h,** Number of *Adar*$^{Zα/-}$ *Mlkl*$^{-/-}$ *Casp8*$^{+/+}$, *Adar*$^{Zα/-}$ *Mlkl*$^{-/-}$ *Casp8*$^{+/-}$ or *Adar*$^{Zα/-}$ *Mlkl*$^{-/-}$ *Casp8*$^{-/-}$ mice that survived beyond day 2 after birth (> P2).

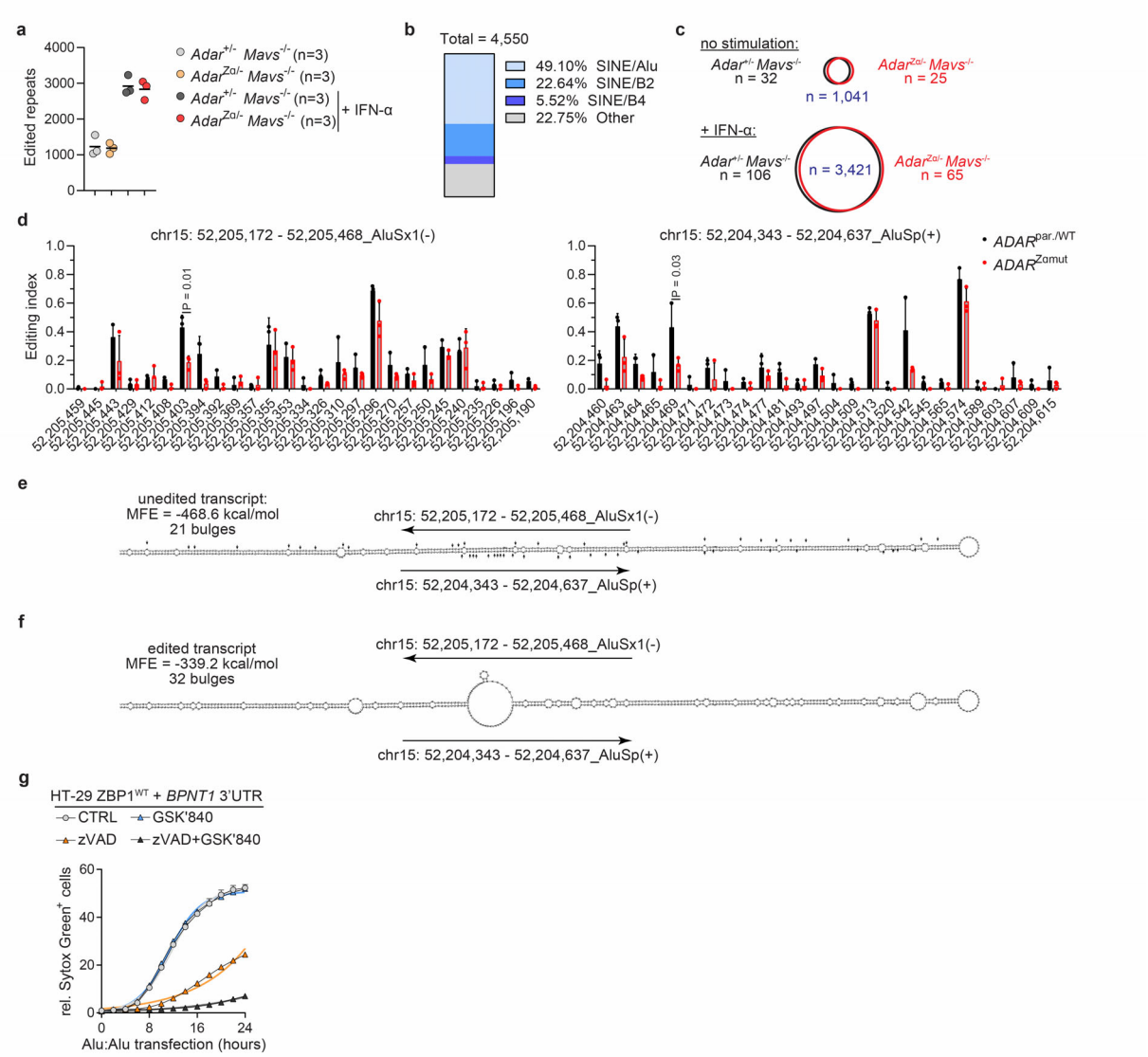

947

948 **Extended Data Fig. 10. A-to-I editing analysis of mRNA in mouse and human ADAR1**
949 **Zα domain mutant cells. a,** Primary lung fibroblasts derived from mice of the indicated
950 genotypes were stimulated for 16 hours with 200 U/mL IFN-α or left untreated. The total
951 number of murine repeat elements that underwent A-to-I editing was determined for 3
952 independent cell lines per genotype. Lines represent the mean. **b,** Boxplot illustrating the
953 distribution of repeat elements in which editing activity was observed in 3 individual cell lines
954 per genotype treated or not with IFN-α as indicated in **(a)**. **c,** Venn diagrams displaying the
955 number of repeat elements of which A-to-I editing activity was restricted to a single genotype
956 (*Adar*$^{+/-}$ *Mavs*$^{-/-}$ or *Adar*$^{Zα/-}$ *Mavs*$^{-/-}$) or those that were detected in both groups without

957 stimulation or following IFN-α treatment as indicated in **(a)**. **d,** Graphical representation of
958 the differential A-to-I editing profile of *ADAR*$^{Par/WT}$ and *ADAR*$^{Z\alpha mut}$ HEK293 cells detected on
959 the indicated AluSp element in Fig. 4c and its nearest inverted repeat element (AluSx1). Data
960 points show mean + SD; P values by Welch's t-test. **e,f,** The RNAfold webtool was used to
961 predict the folding structure and minimum free energy (MFE) of dsRNA formed by the
962 AluSp:AluSx1 hybrid in complete absence of A-to-I editing **(e)** and when fully edited **(f)** at
963 the A-to-I sites identified in **(d).** The A-to-I editing sites are indicated with black arrows. **g,**
964 Transfection of HT-29 ZBP1^{WT} with 50 ng of *BPNT1* 3'UTR duplex RNA in combination
965 with 3 μM GSK'840 and/or 20 μM zVAD-fmk. Cell death was analysed as in Fig. 3d. Fitted
966 lines represent a logistic growth fit. Data points show the mean of 2 technical replicates + SD
967 and are representative of 3 independent experiments.
968